The role of innate cell differentiation in promoting *yki*$^{3S/A}$ intestinal tumor cell invasiveness and defining the systemic cachexia-like wasting phenotypes

Inez Keiko Arlyne Pranoto

A dissertation
Submitted in partial fulfillment of the
requirements for the degree of

Doctor of Philosophy

University of Washington
2023

Reading Committee:
Young Kwon, Chair
James Hurley
Richard Palmiter

Program Authorized to Offer Degree:
Biochemistry

©Copyright 2023
Inez Keiko Arlyne Pranoto

University of Washington

Abstract

The role of innate cell differentiation in promoting *yki*$^{3S/A}$ intestinal tumor cell invasiveness and defining the systemic cachexia-like wasting phenotypes

Inez Keiko Arlyne Pranoto

Chair of the Supervisory Committee:
Young Kwon
Department of Biochemistry

Many tumors recapitulate the developmental and differentiation program of their tissue of origin, a basis for tumor cell heterogeneity. Although stem-cell-like tumor cells are well-studied, the roles of tumor cells undergoing differentiation in inducing the phenotypes associated with advanced cancers remains to be elucidated. Here, we employ *Drosophila* genetics to demonstrate that the native differentiation program of intestinal stem cells plays a key role in determining an intestinal tumor's capacity to invade and induce various non-tumor-autonomous phenotypes. The differentiation program that generates absorptive cells called enterocytes is aberrantly recapitulated in the intestinal tumors generated through activation of the Yap1 ortholog Yorkie. Elimination of tumor cells in the enterocyte lineage allows stem cell-like tumor cells to grow but suppresses invasiveness and reshapes various phenotypes associated with cachexia-like wasting by altering the expression of tumor-derived factors. Meanwhile, enriching the intermediately differentiated tumor cells in the enterocyte lineage promotes a more robust and quicker tumor growth that lacks cell invasive properties but enhances tumor-derived factors expression, resulting in a more advanced manifestation of cachexia-like wasting syndrome in the host. This study provides insight into how a native differentiation program determines a tumor's capacity to induce the phenotypes associated with advanced cancers and suggests that manipulating the differentiation programs co-opted in tumors might be a way to treat some complications of cancer, including cachexia.

Contents

List of Figures

Acknowledgments

Right after passing my PhD candidacy exam, every time I listened to the acknowledgement part of a dissertation, I would start tearing up at the thought of the people that I'm grateful for. As it's finally my time to write this section for my dissertation, I, once again, found myself on the brink of tears, overwhelmed with emotions and memories from the past six years. Pursuing a path in a PhD program has been the most intellectually stimulating, emotionally challenging, and character defining journey that truly shapes who I am as a scientist and, more importantly, as a person. Throughout this unique experience, I am lucky to have a long list of people that continue to support me in various ways.

I'd like to begin with the person that brought the idea of joining a PhD program into my head, my thesis advisor, Young Kwon. Young has consistently been generous with his time and patient at teaching me how to creatively design experiments, how to thoroughly interpret data analysis from all angles, and how to manage and regroup my thoughts when experiments did not go as planned or when new evidence did not support my hypotheses. Through his examples and gazillion feedbacks, he also has helped me to improve on my public speaking skill and how to deliver and tailor my presentations to capture the attention of audience with varying science background. More importantly, throughout his mentorship, he has been a strong, yet calm mentor who has taught me invaluable lessons on how to navigate hardships in graduate school, especially those beyond doing scientific research, how to move on from mistakes and failures, and grow from them. These scientific and interpersonal skills that might have been tough pills to learn have given me confidence to face new challenges and whatever may come next in my career. Above all, thank you for believing in me especially when I couldn't, and for continuing to push my limit.

Shout out to the people in the Kwon lab: Jiae Lee, Akimi Green, Annabel Vernon, Alejandra Cabrera, Hyungjoon Park, Ken Dombek, and Semi Hong. Unfortunately, my beloved flies don't pause their lives so I can enjoy my weekend or holidays, which often led me to spend those days in the lab. But I can always count on this hardworking, driven bunch to also be there and provide emotional support through camaraderie. Thank you all for fostering such an encouraging and nurturing environment to work in, for always being ready to help each other, and for always being so willing to try my random ideas, like making matching lab t-shirts or starting weekly lab meetings by sharing a roundtable high and a low moment of the week. I will absolutely miss our annual Winter parties, lab dinner hangouts, and organizing

lab outings in the summers. I especially would like to thank Jiae, whom I highly look up to, for being such a good mentor, friend, and my first beer buddy. So much of my work ethics, probing question skills, experimental design skills, and professional soft skills have been modeled after hers and I cannot ask for a better second mentor. To Akimi, my perpetually bubbly and sweet bench mate, thank you for putting up with my random heavy sighs and grunts during those abysmal revision months. To Annabel, whom I secretly admire for her calm composure, her thoroughness, and her tenacity in reading papers, thank you for setting a good example for me to improve as a graduate student and as a scientist.

I am grateful for the people in my Biochemistry/BPSD 2017 cohort and those whom I met through them: Gabi Reggiano, Ryan Kibler, Olivia Thibeault, Halli Benasutti, Robby Divine, Mimi Divine, Carson Adams, Meg Adams, and James Griffin. Thank you for continuing to choose to stick together and for putting the time and effort to maintain our friendship beyond our first year, when we did not have to be in the same space on campus as much anymore. These people introduced me to so many new things that I wouldn't have thought of doing, like renting a small boat on SLU and incessantly waving at every passing boat, going to a happy hour at Pacific Science Center where the influence of alcohol brought out the child in us, and staying in a very weirdly-themed "cabin" (it's a purple painted castle with lots of dragons and knights decorations, among other things, and a trick wall-height painting that leads to a storage cabinet). Little did I know how much support they provided merely by fighting through graduate school along with me. Special thanks to Ryan and Olivia for keeping me sane, especially during the tail end of graduate school, and for helping me shrug my FOMO for being the last one out in the group.

I want to especially thank Irini Topalidou, Amy Bounds, Gabi Reggiano, and Celia Bisbach. They made graduate school less isolating and provided great comfort and endless support, particularly during the last few months of graduate school. To Irini, whom I met when I was an undergraduate research assistant and who has been by my side ever since, with your kindness, hopefulness, and overall positivity, you have taught me to how to find the silver lining in every difficult situation. Thank you for always seeing the good in me, even at my lowest moments. To Amy, the unexpected friend I made from the student buddy program, thank you for keeping your ears open for me, for always making me feel understood and for being a reminder that working hard and having fun outside of work is something attainable during graduate school. She is one of the few reasons I'm not at work 7 days a week,

especially this past year. To Gabi, who never fails to remind me of my achievements and what I'm good at. Little did I know how much weights our Saturday night hang out sessions hold in balancing my intense work habit. Thank you for being my buddy throughout graduate school and making it fun and less lonely. Celia, with her logical, yet empathetic approach, has always inspired me to be courageous in facing new challenges, dealing with the unexpected, and accepting differences in navigating science and life. Thank you for continuing to cheer me on and for always being there for me despite the time difference and 2,000 miles separation. Words can't fully capture how grateful I am to have met these people in graduate school and I just can't wait for our next ventures beyond graduate school.

And to Nadya Lumanpauw. I'm so fortunate to have found her in college as a friend to confide in and together, fight through the struggle of being away from home and figuring out adulthood in a foreign land. Despite my bottomless pit of anxieties throughout graduate school, Nadya has always been by my side with her endless support and helped me not to overlook the personal growth and the lessons I have learned by being in graduate school, especially when I fail to recognize them myself. Thank you and I'm excited to continue exploring our next life chapter wherever we will be.

Lastly, to my family. Thank you for having faith in me and just letting me be to pursue something so uncommon and so unfamiliar. I know how terrifying it could be to see me committing 6 years of my life to a program that is conceptually so abstract. Thank you for staying back and watching me go after my career dream. I can't wait to have more time to chat or take that 22-hour flight back home and hang out with my mama.

Dedication

This thesis dissertation is the fruit of a work that I dedicated my twenties to.

Let this be a written reminder that nobody except yourself should and could define your limit.

Chapter 1: Introduction

Division of stem cells and their differentiation processes generate the heterogeneous cell populations required for tissue development and maintenance (Hwang et al., 2008; Jiang et al., 2016; Jiang & Edgar, 2009; Krieger & Simons, 2015; Micchelli & Perrimon, 2006; Ohlstein & Spradling, 2006; Zakrzewski et al., 2019). Recent studies employing single-cell sequencing strategies have highlighted the striking cellular heterogeneity of human cancers and mouse cancer models (Couturier et al., 2020; Goveia et al., 2020; N. Kim et al., 2020; Lawson et al., 2018; Wu et al., 2021; Yeo et al., 2020). Several human cancers have been shown to recapitulate the developmental and/or differentiation programs that form and maintain the tissues of origin (Borczuk et al., 2003; Couturier et al., 2020; Fukuzawa et al., 2017; Goveia et al., 2020; Kelleher et al., 2006; Wu et al., 2021). Interestingly, Genovese et al. have shown that the temporal patterning program is partially co-opted in *Drosophila* neuroblast tumors (Genovese et al., 2019). Along with the concept that dedifferentiation is associated with malignancy, the roles of cancer-cell populations with stem-cell-like properties have been extensively studied (Chen et al., 2013; da Silva-Diz et al., 2018; Jögi et al., 2012). It remains to be determined, however, how these developmental and differentiation programs that are recapitulated in cancers contribute to the various phenotypes associated with advanced cancers, including metastasis and cachexia, most of which are responsible for the mortality of cancer patients.

Oncogenes do not elicit the same tumorigenicity and tumor-related phenotypes across different tissues (Cook et al., 2021; Figueroa-Clarevega & Bilder, 2015; Kwon et al., 2015; J. Lee et al., 2020; Lowell et al., 2000; Pagliarini & Xu, 2003; Rangarajan et al., 2001; Tu et al., 2019; Weng et al., 2006; Yang et al., 2019), implying that the characteristics of cancers cannot be attributed entirely to the alterations in their genome. Similarly, in *Drosophila*, expression of an oncogene often gives rise to different phenotypes in the imaginal discs–the developing epithelia inside larvae–and the adult midgut epithelium. Expression of activated forms of the Yes-associated protein 1 (Yap1) oncogene ortholog *yorkie* (*yki*), such as yki^{S168A} and $yki^{3S/A}$, is sufficient to drive uncontrolled cell division in multiple epithelial tissues, resulting in the formation of hyperplasia (hereafter, *Drosophila* 'tumors') (Kwon et al., 2015; Oh & Irvine, 2009; Pan, 2010; Wang et al., 2016; Wittkorn et al., 2015). Transplantation of yki^{S168A} imaginal disc

tumors into adult flies does not induce wasting in the host tissues even though the transplanted tumors grow large inside the hosts (Figueroa-Clarevega & Bilder, 2015). In contrast, formation of *yki*$^{3S/A}$ tumors in the midgut epithelium induces cachexia-like wasting, manifested by ovary atrophy, muscle degeneration, and metabolic abnormalities (Kwon et al., 2015). Additionally, while imaginal disc tumors generated by activation of Yki are not metastatic, our observations show that a portion of *yki*$^{3S/A}$ midgut tumor cells and *yki*^{S168A} midgut tumor cells can migrate out of the midgut across the visceral muscle (VM). These observations suggest that the malignant phenotypes caused by activated Yki midgut tumors cannot be attributed solely to the overexpression of these oncogenes. I speculate that midgut-specific contextual information might play a role in eliciting these phenotypes. In this study, we attempted to address how the invasive and the cachexia-like wasting phenotypes arise in *yki*$^{3S/A}$ midgut tumors to gain insights into how the physiology of the tissue of origin contributes to a tumor's ability to induce malignant phenotypes.

While the epithelial cells in imaginal discs are relatively homogenous, the intestinal epithelium comprises 4 cell types: intestinal stem cells (ISCs), enteroblasts (EBs), enterocytes (ECs), and enteroendocrine cells (EEs) (Boumard & Bardin, 2021; Hou & Singh, 2017; Jiang et al., 2016; Micchelli & Perrimon, 2006; Miguel-Aliaga et al., 2018; Ohlstein & Spradling, 2006). ISCs are the diploid cells expressing Delta (Dl)–the ligand of the Notch (N) signaling pathway. ISCs divide and by default generate themselves while activation of Notch signaling makes ISCs generate their progenitor cells EBs (Boumard & Bardin, 2021; Hou & Singh, 2017; Jiang et al., 2016; Micchelli & Perrimon, 2006; Miguel-Aliaga et al., 2018; Ohlstein & Spradling, 2006). Subsequent activation of Notch signaling in EBs triggers differentiation of EBs into ECs, which are the absorptive polyploid cells (Micchelli & Perrimon, 2006). ISCs also give rise to a distinct EE lineage (Biteau & Jasper, 2014; Zeng & Hou, 2015) (Fig. 1). The midguts generate intermediately differentiated EBs, which then migrate and terminally differentiate to replace damaged ECs, a process requiring epithelial-mesenchymal transition (EMT) followed by mesenchymal-epithelial transition (MET). A snail family EMT transcription factor, *escargot* (*esg*), plays a key role in EC differentiation (Antonello, Reiff, & Dominguez, 2015; Korzelius et al., 2014; Loza-Coll et al., 2014). ISCs express less *esg* compared to EBs, which suggests that ISCs are in a partial EMT state while EBs elicit a full EMT state (Antonello, Reiff, & Dominguez, 2015). Indeed, the differentiating EBs show the morphological features of mesenchymal cells and the ability to migrate (Antonello, Reiff, & Dominguez,

2015). Note that stem cells can also migrate upon tissue damage (Hu et al., 2021). ***Although midgut tumors can be generated by expressing oncogenes in ISCs and EBs*** (Apidianakis et al., 2009; J. Lee et al., 2021; Markstein et al., 2014), ***it is not clear whether the normal differentiation programs are recapitulated in these tumors to generate a heterogeneous population of tumor cells. Furthermore, it remains underexplored how a differentiation program recapitulated in tumors or how a population of tumor cells undergoing differentiation contributes to the expression of the various advanced tumor phenotypes in Drosophila as well as in humans.***

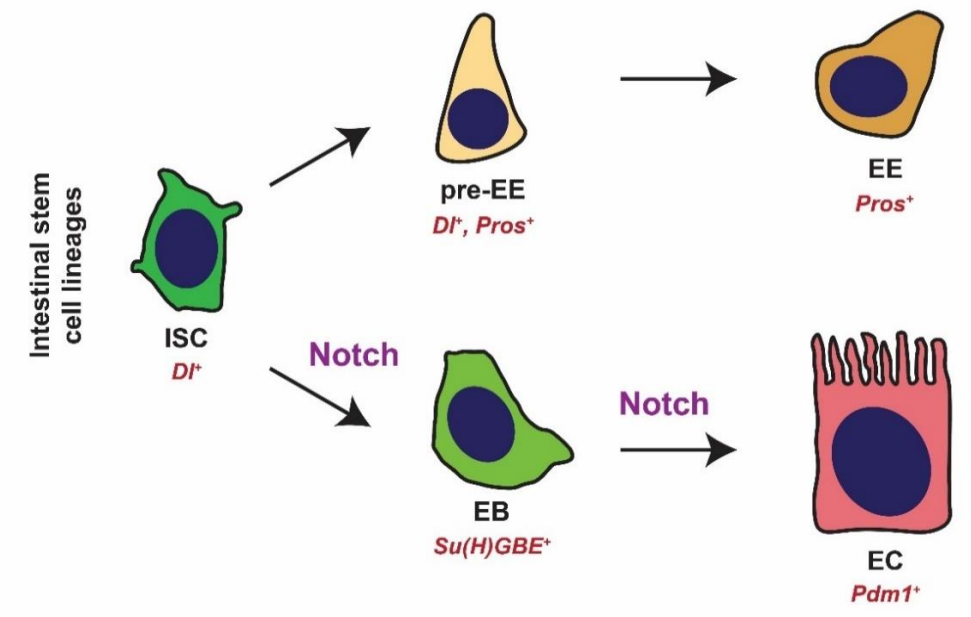

Figure 1. Intestinal cell differentiation programs in adult *Drosophila* midgut yields heterogeneous cell population in the intestinal epithelium.
Intestinal stem cells (ISC) can differentiate into pre-enteroendocrine cells (pre-EE), which eventually become enteroendocrine cells (EE). ISC can also undergo a distinct differentiation lineage, initiated by high Notch signaling activation, to become progenitor enteroblast cells (EB), which then terminally differentiate into enterocytes cells (EC). Each cell type expresses unique cell markers as listed in red. ISC cells are marked with *Delta* (*Dl*) marker, pre-EE cells are positive for both *Dl* and *Prospero* (*Pros*) markers, EE cells express *Pros* marker, EB cells are positive for *Su(H)GBE* marker, and EC cells are marked with *Pdm1*.

In this thesis study, we attempted to provide insights on these conundrums by studying adult *Drosophila* $yki^{3S/A}$-induced midgut tumors. Our characterization revealed a striking heterogeneity among these $yki^{3S/A}$ cells derived from an aberrant reconstitution of EC-lineage cell differentiation program. Besides enriching its cell heterogeneity composition, as $yki^{3S/A}$ midgut tumor becomes more advanced, a

subpopulation of *yki*$^{3S/A}$ cells exhibited invasive properties and manifested cachexia-like wasting phenotypes in the host. By genetically manipulating the EC-lineage differentiation in *yki*$^{3S/A}$ tumor cells, we illustrated that maintaining the EC differentiation program, which gives rise to high tumor cell heterogeneity, was crucial for the ability of *yki*$^{3S/A}$ cells to disseminate from the midguts and to define the symptoms of non-tumor-autonomous phenotypes in tumor host. This study provides insights into how the contextual information in the tissue of origin can give rise to a unique tumor-cell composition, which results in tumor's capacity to induce the phenotypes associated with invasiveness and cachexia-like wasting phenotypes.

Chapter 2: *yki*$^{3S/A}$ tumors accumulate aberrantly heterogeneous cells in the EC lineage

Expression of an active form of *yki* (*yki*$^{3S/A}$) in adult ISCs and EBs using the conditional GAL4 driver *esg*^{ts} (*esg-GAL4*, *tub-GAL80*^{ts}, *UAS-GFP*/+; see Methods) resulted in the development of hyperplastic midgut tumors (Fig. 2.1A).[1] However, despite overexpressing the same oncogene, the size of *GFP*+ tumor cells in *yki*$^{3S/A}$ midgut tumors are widely variable, suggesting that *yki*$^{3S/A}$ cells were not a homogeneous population (Fig. 2.1B). During normal differentiation of EBs into ECs, EBs increase their size and ploidy. In contrast, EEs are generally smaller. Therefore, we hypothesized that measuring their nuclear size might be a way to investigate the heterogeneity of *yki*$^{3S/A}$ cells.

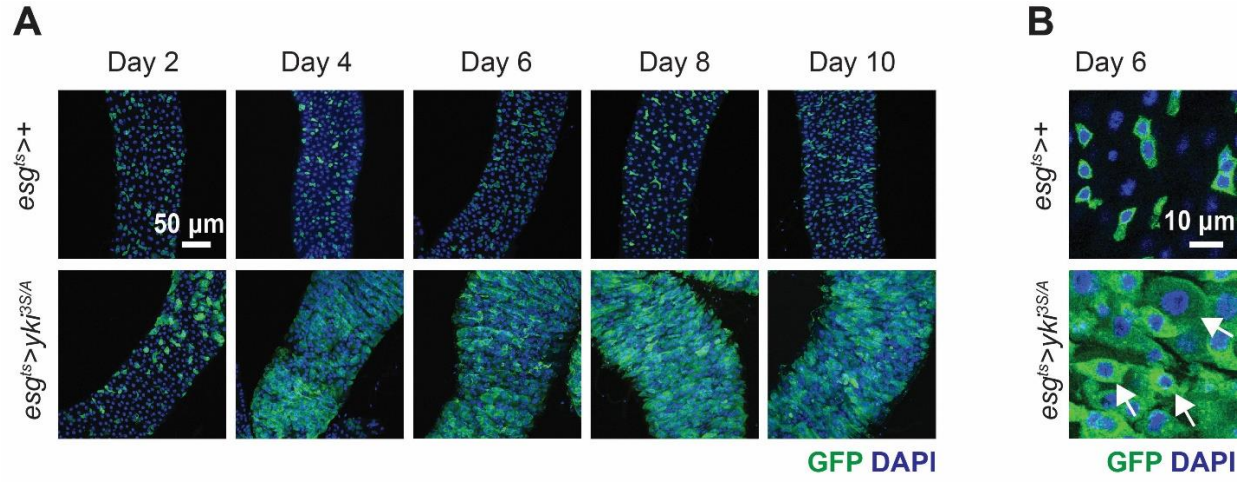

Figure 2.1. Expression of *yki*$^{3S/A}$ in ISC and EB cells using *esg*^{ts} induces hyperplastic midgut tumor enriched in tumor cell heterogeneity.
A. Posterior region of *esg*^{ts}>+ and *esg*^{ts} >*yki*$^{3S/A}$ midguts. *yki*$^{3S/A}$ was expressed with *esg*^{ts} by shifting to 29°C for the indicated durations. The cells manipulated by *esg*^{ts} are marked with GFP (green), and nuclei are stained with DAPI (blue). **B**. *yki*$^{3S/A}$ tumor cells are highly heterogeneous in size. Arrows point to different sizes of GFP+ cells in *yki*$^{3S/A}$ tumor.

[1] As mentioned in Chapter 1, there are two activated forms of *yki* oncogenes, *yki*^{S168A} and *yki*$^{3S/A}$. Expression of *yki*^{S168A} with *esg*^{ts} (*esg*^{ts}>*yki*^{S168A}) also induced hyperplastic midgut tumors with similar tumor cell composition to *yki*$^{3S/A}$ tumor cells, but *esg*^{ts}>*yki*^{S168A} tumors grow more slowly than *esg*^{ts}>*yki*$^{3S/A}$ tumors (Fig. S1A, C, D). We also observed cell dissemination phenotype (an invasive phenotype that will be discussed in Chapter 3) in *yki*^{S168A} cells, although fewer and much later in tumor development compared to *yki*$^{3S/A}$ cells (Fig. S1B). Hence, in this thesis project, we focused on *esg*^{ts}>*yki*$^{3S/A}$ midgut tumors.

In control midguts, *esg*^{ts}-driven GFP marks ISCs and EBs, which are *esg*$^{+}$ cells; ECs and EEs are not *esg*$^{+}$ or *GFP*$^{+}$. Likewise, *esg*^{ts}-driven GFP marks *yki*$^{3S/A}$ cells. The nuclear size measurement of *esg*$^{+}$ cells in the control posterior midguts revealed three peaks (Fig. 2.2A, indicated with brackets and designated as I, II, and III). The main peak (I) was detected at around 11-15 μm^2, followed by a nuclei population (II) at around 19-23 μm^2 (Fig. 2.2A). Additionally, relatively small nuclei formed a small peak (III) at around 6-9 μm^2 (Fig. 2.2A). To understand how ISCs and EBs contribute to the overall distribution of *esg*$^{+}$ nuclei, we also quantified the nuclear size of cells marked by *Dl*$^{+}$—an ISC marker— or *Su(H)GBE*$^{+}$—an EB marker. Interestingly, the *Su(H)GBE*$^{+}$ nuclei size distribution showed a major peak at 11-15 μm^2 and a second major population with larger nucleus approximately at 19-23 μm^2 (Fig. 2.2A', shown by brackets), which were reminiscent of the peaks I and II in the *esg*$^{+}$ nuclear size distribution. The nuclear size distribution of *Dl*$^{+}$ cells showed two peaks at 6-9 μm^2 and 11-15 μm^2 (Fig. 2.2A'', indicated by brackets), which could be overlayed with the peaks III and I in the *esg*$^{+}$ nuclear size distribution, respectively. These data suggest that both ISCs and EBs can contribute to the peak I while EBs and ISCs mainly contribute to the *esg*$^{+}$ peak II and the *esg*$^{+}$ peak III, respectively. I also measured the nuclear size of *esg*$^{-}$ cells, which revealed two well-separated populations (Fig. S2A, arrows). Measuring the nuclear size of EEs, which are marked by an EE marker *prospero* (*pros*), showed a population of small nuclei (Fig. S2B) reminiscent of the *esg*$^{-}$ small nuclei population at 6-9 μm^2. Thus, we concluded that the large *esg*$^{-}$ nuclei population represented ECs (Fig. S2A). Interestingly, the *esg*$^{+}$ peak III overlapped with the distribution of EE nuclei, which raised the possibility that the *esg*$^{+}$ peak III might represent a population of *esg*$^{+}$ cells in the EE lineage. Notably, the larger *Su(H)GBE*$^{+}$ population can be placed between the *esg*$^{+}$ peak I and the EC nuclei peak at around 30 μm^2, suggesting that the *esg*$^{+}$ and *Su(H)GBE*$^{+}$ populations with larger nucleus might represent differentiating EBs. These analyses demonstrate that measuring nuclear size can be a way to assess the heterogeneity of midgut epithelial cells.

Given these results, we attempted to describe the population of *yki*$^{3S/A}$ cells by measuring their nuclear size. As expression of *yki*$^{3S/A}$ with *esg*^{ts} significantly increased cell division, significantly more *GFP*$^{+}$ cells (11.83±0.35 cells per 50 μm x 50 μm region) were detected from a selected area in *yki*$^{3S/A}$ midguts compared to control midguts (5.65±0.17 cells per 50 μm x 50 μm region). Although *yki*$^{3S/A}$ nuclei were also populated at 11-15 μm^2, we observed a peak afterward (Fig. 2.2B, arrow) and a huge

population of cells with strikingly large nuclei (Fig. 2.2B, bracket). Assuming that the population at 11-15 μm^2 represents the majority of "normal" ISCs and EBs in control epithelium, we decided to use the 11-15 μm^2 population as an internal reference to bin the data by 4 μm^2, starting from 11 μm^2, to calculate the population sizes relative to the population at 11-15 μm^2 in each genotype (Fig. 2.2C-C''). This revealed a shift in the major cell population to 15-19 μm^2 and a clear increase in the larger esg^+ nuclei population in $yki^{3S/A}$ midguts compared to control midguts (Fig. 2.2C). Additionally, we observed an increase in the population of $Su(H)GBE^+$, $yki^{3S/A}$ cells with larger nucleus (>15 μm^2), which might represent differentiating EB-like cells (Fig. 2.2B' and C'). Intriguingly, large Dl^+ nuclei (>15 μm^2) were more abundant in $yki^{3S/A}$ midguts (Fig. 2.2B'' and C''). Therefore, accumulation of both large $Su(H)GBE^+$ and Dl^+ nuclei accounts for the increase in the lagging population of $yki^{3S/A}$ nuclei. Unexpectedly, a significant portion of $Su(H)GBE^+$, $yki^{3S/A}$ nuclei were determined to be even larger than normal EC nuclei (Fig. 2.2B' and D). Similarly, we also detected Dl^+, $yki^{3S/A}$ nuclei even larger than normal EC nuclei (Fig. 2.2B'' and E). Strikingly, we found that a subpopulation of the $Su(H)GBE^+$, $yki^{3S/A}$ cells were also Dl^+ (Fig. 2.2F), suggesting a prolonged hybrid state of ISC-EB transition in these Dl^+, $Su(H)GBE^+$ $yki^{3S/A}$ cells. While it appeared that a portion of $yki^{3S/A}$ cells could undergo terminal differentiation as Pdm1 signals – a commonly used EC marker – were detected in a portion of large GFP^+ cells, some small nucleated $yki^{3S/A}$ cells are also positive Pdm1 marker, a distinct cell population that is not typically found in the control intestine (Fig. 2.2G). Previous studies have shown that driving ISC differentiation towards ECs causes a reduction in EE cells (Beebe et al., 2010; Zeng & Hou, 2015). Indeed, EE cells were less frequently detected in regions where $yki^{3S/A}$ cells were populated, implying that EE differentiation is reduced by the expression of $yki^{3S/A}$ (Fig. S3A and B). These observations suggest that $yki^{3S/A}$ midguts still maintain the EC differentiation program even though it is not normal, resulting in an accumulation of a variety of cell populations, including aberrantly differentiating EB-like cells (Fig. 2.3).

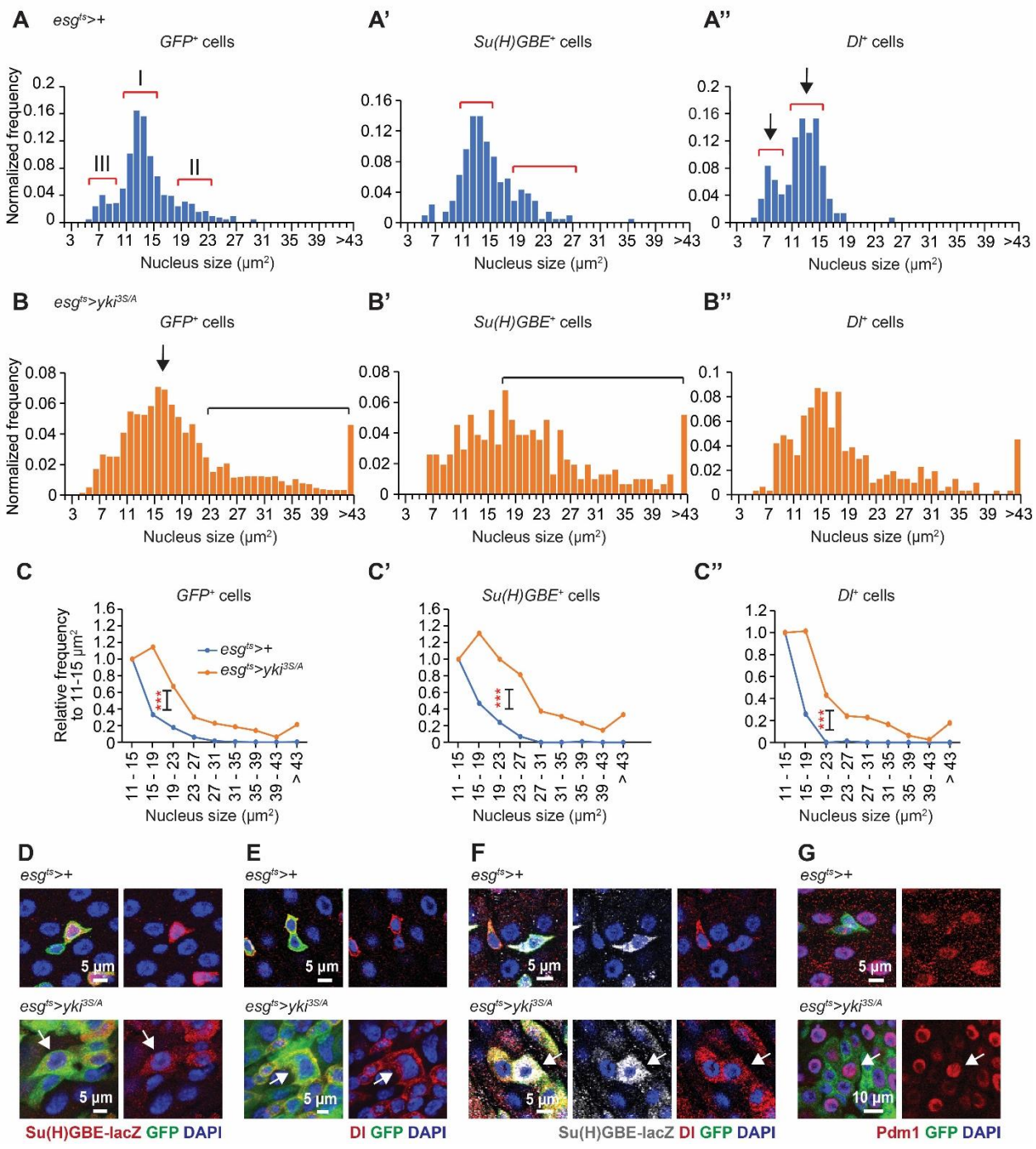

Figure 2.2. The EC differentiation program is aberrantly recapitulated in *yki$^{3S/}$*midgut tumors, leading to generation of heterogeneous types of *yki$^{3S/A}$* cells.

A-A''. Nuclear size distribution of *GFP*$^+$ cells (A), *Su(H)GBE*$^+$ cells (**A'**), and *Dl*$^+$ cells (**A''**) in control (*esg^{ts}*>+) midguts at day 6 of transgene induction. Numbered red brackets in (**A**) indicate three different cell populations described in the text. **B.** Nuclear size distribution of GFP$^+$ cells (**B**), *Su(H)GBE*$^+$ cells (**B'**), and *Dl*$^+$ cells (**B''**) in *esg^{ts} >yki$^{3S/A}$* midguts at day 6 of transgene induction. **C-C''.** Normalized Nuclear size distribution. Transgenes were induced for 6 days. The data is binned by 4 μm starting from 11 μm. Normalized frequency shows the population sizes relative to the population at 11-15 μm.

GFP^{+} cells (**C**), N=691 (*esg*^{ts}>+) and N=1869 (*esg*^{ts}>*yki*$^{3S/A}$); *Su(H)GBE*$^{+}$ cells (**C''**), N=179 (*esg*^{ts}>+) and N=265 (*esg*^{ts}>*yki*$^{3S/A}$); *Dl*$^{+}$ cells (**C''**), N=103 (*esg*^{ts}>+) and N=264 (*esg*^{ts}>*yki*$^{3S/A}$). ***P<0.001, Chi-Square test. **D.** *Su(H)GBE-lacZ* staining of posterior midguts at day 6. GFP marks *esg*$^{+}$ cells (green). Arrow indicates a representative large *Su(H)GBE*$^{+}$, *yki*$^{3S/A}$ cell. **E.** Dl staining of posterior midguts at day 6. Arrow points to a representative extremely large *Dl*$^{+}$, *yki*$^{3S/A}$ cell. **F.** Dl and *Su(H)GBE-lacZ* co-staining of midguts at day 6. Arrow indicates a representative *Dl*$^{+}$, *Su(H)GBE*$^{+}$, *yki*$^{3S/A}$ cell. **G.** Pdm1 staining of posterior midgut at day 6. Arrow points a representative *GFP*$^{+}$, *Pdm1*$^{+}$, *yki*$^{3S/A}$ cells.

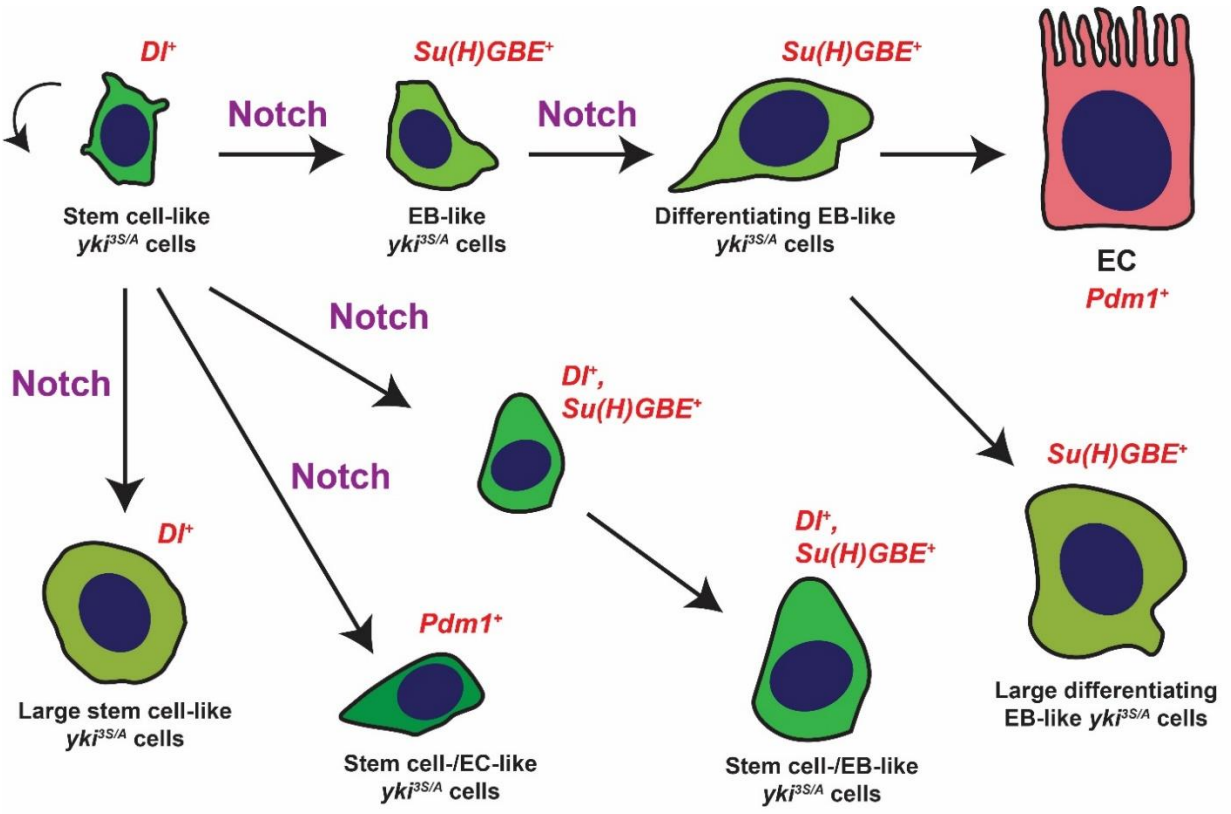

Figure 2.3. Summary of the cell heterogeneity among *yki*$^{3S/A}$ midgut tumor cells.
Based on immunofluorescence data, while some *yki*$^{3S/A}$ cells are in the typical cell states found in the control intestine (top row), many *yki*$^{3S/A}$ cells are in hybrid cell states along the EC-lineage differentiation program, resulting in an overall higher cell heterogeneity in *yki*$^{3S/A}$ midgut tumor.

Chapter 3: A population of *yki*$^{3S/A}$ cells show invasive properties

3.1. A portion of *yki*$^{3S/A}$ cells basally disseminate from the posterior midguts

Previous studies in the lab showed that expression of a mutant *Ras* (*Ras*^{V12}) in adult ISCs and EBs using the conditional GAL4 driver *esg*^{ts} could induce tumors in the midguts for a short period but at day 2 of *Ras*^{V12} expression, they basally disseminate and apically delaminate, resulting in a removal of most of *Ras*^{V12} cells from the posterior midguts (J. Lee et al., 2020). In contrast, expression of *yki*$^{3S/A}$ with *esg*^{ts} (*esg*^{ts}>*yki*$^{3S/A}$) resulted in midgut tumors which persist over time (Fig. 2.1A). Unlike *Ras*^{V12} cells at day 2, *yki*$^{3S/A}$ cells showed strong Armadillo (Arm)–the *Drosophila* β-catenin ortholog–signals at the cell-cell junctions, an indication of intact adherens junctions (Fig. 3.1A). Moreover, overall Arm signals were significantly increased in *yki*$^{3S/A}$ cells compared to control *esg*$^{+}$ cells (ISCs and EBs) (Fig. 3.1A and B). Consistently, most of the *yki*$^{3S/A}$ cells stayed at the epithelium, and apical delamination of *yki*$^{3S/A}$ cells was not frequently observed (Fig. 3.1C). Strikingly, a significant number of *yki*$^{3S/A}$ cells were also detected outside of the visceral muscle (VM) at the posterior midguts as early as day 4 of *yki*$^{3S/A}$ expression, a phenotype that became more robust over time (Fig. 3.1D and E). These observations indicate that a portion of *yki*$^{3S/A}$ cells can invade and migrate out from the midguts across the VM and the extracellular matrix (ECM) while most of *yki*$^{3S/A}$ cells stay in the epithelium.

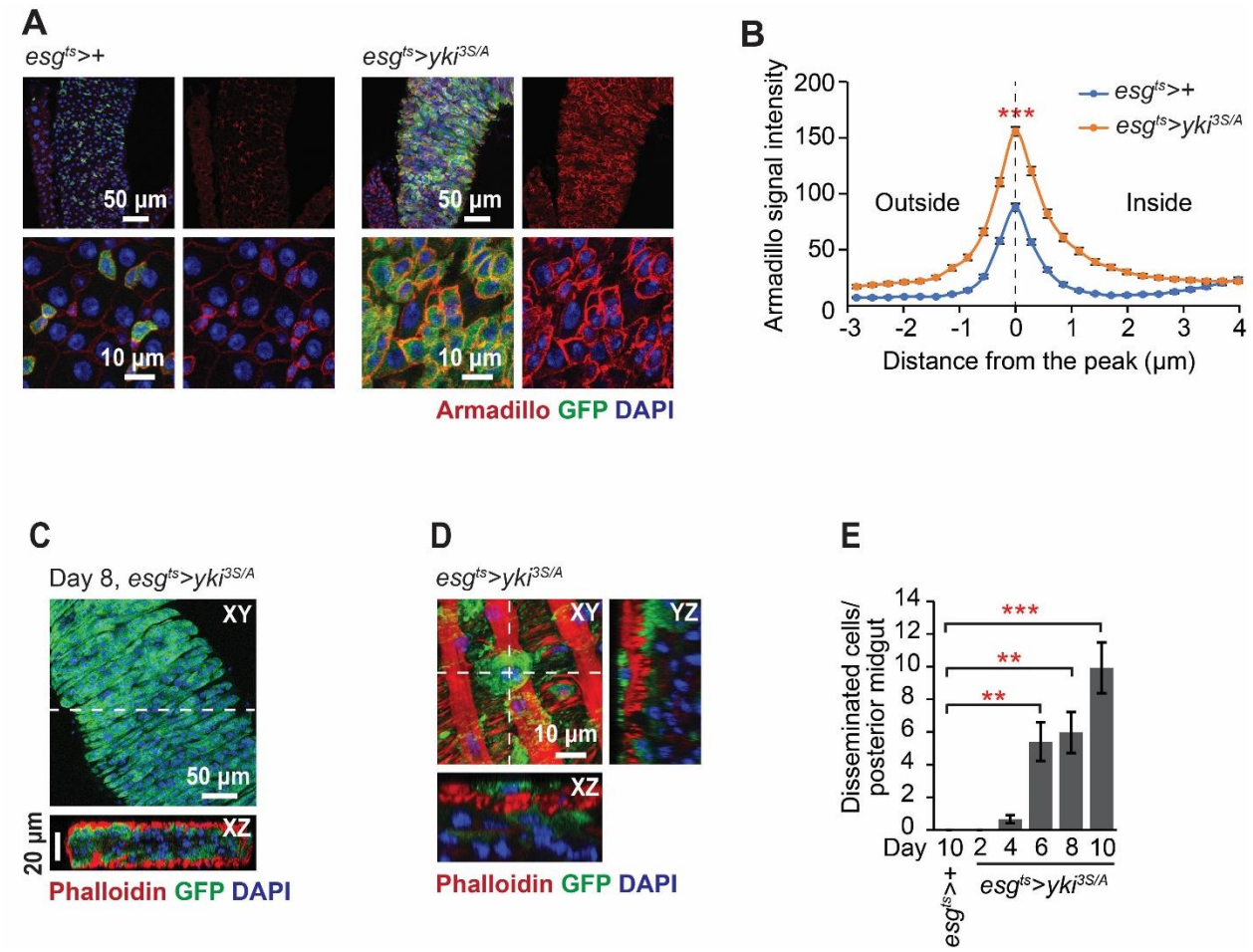

Figure 3.1. Some cells in yki$^{3S/A}$-induced midgut hyperplasia disseminate from the midguts.
A. Arm signals (red) in the posterior midguts. Transgenes were induced 6 days using *esg-GAL4, UAS-GFP, Tub-GAL80^{ts}* (*esg^{ts}*) by shifting to 29°C. Cells manipulated by *esg^{ts}* are marked by GFP (green). Nuclei were stained by DAPI (blue). **B.** Quantification of Arm signals in *GFP^{+}* cells. Transgenes were induced for 6 days. N=125 cells from 5 midguts, *esg^{ts}>+*; N=145 cells from 7 midguts, *esg^{ts}>yki$^{3S/A}$*. Mean±SEMs are shown, ***P<0.001, two-tailed unpaired Student's t-test at distance = 0 µm. **C.** Representative orthogonal views of the posterior midguts at day 8 of induction. **D.** Representative image of disseminated *yki$^{3S/A}$* cell. Top and orthogonal views are shown. Phalloidin (red) visualizes visceral muscle. **E.** Quantification of disseminated cells. *GFP^{+}* and *DAPI^{+}* cells detected outside the VM layer in the posterior midguts are counted. Transgenes were induced for indicated days with *esg^{ts}*. N=22 midguts (10 days, *esg^{ts}>+*); N=24 (2 days, *esg^{ts}>yki$^{3S/A}$*); N=24 (4 days, *esg^{ts}>yki$^{3S/A}$*); N=32 (6 days, *esg^{ts}>yki$^{3S/A}$*); N=28 (8 days, *esg^{ts}>yki$^{3S/A}$*); N=29 (10 days, *esg^{ts}>yki$^{3S/A}$*). Mean±SEMs are shown, and **P<0.01,***P<0.001 ANOVA test (p<0.001) followed by Tukey's post-hoc test.

3.2. Matrix metalloproteinase 1 (Mmp1) is increased only in a portion of *yki*$^{3S/A}$ cells and most ECs in *yki*$^{3S/A}$ midguts

A relatively thick ECM layer exists at the basal side of the midgut epithelium (Howard et al., 2019; J. Lee et al., 2020). Thus, *yki*$^{3S/A}$ cells need to breach the ECM to disseminate across the VM. To assess if the ECM was compromised by expression of *yki*$^{3S/A}$ with *esg*^{ts}, we stained control and *yki*$^{3S/A}$ midguts with an anti-laminin antibody. In control midguts, one continuous laminin layer was detected at the basal side (Fig. 3.2A). In contrast, expression *yki*$^{3S/A}$ with *esg*^{ts} resulted in a localized partial breach of the laminin layer (Fig. 3.2A, arrows). Next, we assessed Mmp1 levels in control and *yki*$^{3S/A}$ midguts. In control midguts, Mmp1 signals were detected in ECs; *esg*$^{+}$ cells did not show discernable signals (Fig. 3.2B and C). Interestingly, expression of *yki*$^{3S/A}$ with *esg*^{ts} significantly increased Mmp1 signals in ECs in a non-cell-autonomous manner (Fig. 3.2B). Notably, only a portion of *yki*$^{3S/A}$ cells showed elevated Mmp1 signals while Mmp1 signals were unaltered in most of the *yki*$^{3S/A}$ cells (Fig. 3.2C' and C''). Thus, overall Mmp1 signals in *yki*$^{3S/A}$ cells were increased slightly, yet significantly, when compared to those in control *esg*$^{+}$ cells (Fig. 3.2B).

Prior studies have shown that c-Jun N-terminal Kinase (JNK) signaling increases Mmp1 in tumors and during wound healing in *Drosophila* (Ma et al., 2015; Stevens & Page-McCaw, 2012; Uhlirova & Bohmann, 2006). To address whether JNK signaling was associated with the elevation of Mmp1, we assessed JNK signaling using *puc-lacZ,* which expresses nuclear LacZ under the control of the regulatory sequence of *puckered* (*puc*)–a feedback regulator of JNK signaling (Martín-Blanco et al., 1998). we found that *yki*$^{3S/A}$ cells with increased Mmp1 signals showed increased LacZ signals (Fig. 3.2C'') while LacZ signals were rarely detected in control *esg*$^{+}$ cells (Fig. 3.2C). Note that we attempted to address the role of Mmp1 in the dissemination of *yki*$^{3S/A}$ cells by expressing an RNAi against *Mmp1* (*JF01336*) in *yki*$^{3S/A}$ cells under *esg*^{ts} (Glasheen et al., 2009; S. H. Lee et al., 2012). Loss of Mmp1 decreased the growth of *yki*$^{3S/A}$ tumors. Although Mmp1 depletion suppressed laminin degradation and the dissemination of *yki*$^{3S/A}$ cells, the defect in tumor growth likely accounted for the rescue phenotypes (Fig S4). These results show that expression of *yki*$^{3S/A}$ with *esg*^{ts} partially degrades the laminin layer and increases Mmp1. Although expression of *yki*$^{3S/A}$ with *esg*^{ts} significantly increases Mmp1 in most ECs, Mmp1 is elevated only in a

portion of *yki*$^{3S/A}$ cells. Given the role of Mmp1 in invasiveness, these observations indicate that only a portion of *yki*$^{3S/A}$ cells are invasive.

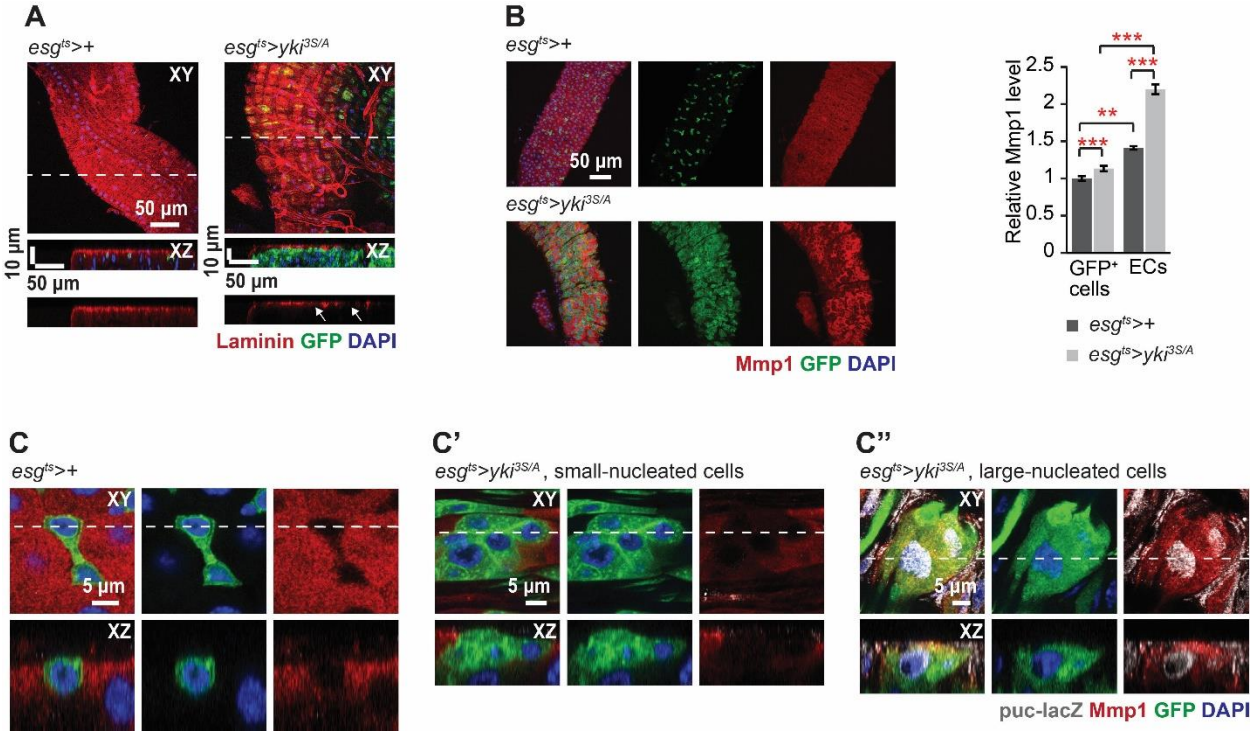

Figure 3.2. Partial and local basement membrane degradation in *yki*$^{3S/A}$ midgut is accompanied with Mmp1 upregulation in the large-nucleated *yki*$^{3S/A}$ cells and the neighboring ECs.
A. Laminin staining (red) of the midguts. Arrows indicate localized degradation of the laminin layer. **B.** Mmp1 staining (red) at 6 days of transgene induction. The graph shows quantification of Mmp1 signals in *GFP*$^{+}$ and EC cells. N=90 cells from 9 *esg*^{ts}>+ midguts; N=110 cells from 11 *esg*^{ts}>*yki*$^{3S/A}$ midguts. Mean±SEMs are shown. *P<0.05, **P<0.01, and ***P<0.001, two-tailed unpaired Student's t-test**. C-C''.** Mmp1 and *puc-lacZ* signals in the midgut epithelia. Representative images of control cells (*esg*^{ts}>+) (**C**), *yki*$^{3S/A}$ cells without Mmp1 and *puc-lacZ* signals (**C')** and *yki*$^{3S/A}$ cells with Mmp1 and *puc-lacZ* signals (**C''**) are shown. In the last panels, both Mmp1 (red) and *puc-lacZ* signals (gray) are shown.

3.3. A portion of *yki*$^{3S/A}$ cells form protrusions across the VM, which are enriched for focal adhesion components

Our previous studies revealed that *Ras*^{V12} cells form bleb-like protrusions, which penetrate the VM by compromising the VM integrity (J. Lee et al., 2020). In contrast, here we found that only a portion of *yki*$^{3S/A}$ cells formed elaborated protrusions while the majority did not (Fig. 3.3B-B''). Additionally, these protrusions transversed the VM layer through the gaps between circular muscles without compromising

the integrity of the tissue (Fig. 3.3A), suggesting that these protrusions are distinct from the bleb-like protrusions observed in *Ras*^{V12} cells.

During migration, cells often assemble focal adhesions at the leading edge, which serve as attachments for dragging the lagging cell bodies (Krakhmal et al., 2015; Pandya et al., 2017). To address whether focal adhesions were assembled at the protrusions transversing the VM, we first checked the localization of integrin–the transmembrane component of focal adhesions. In control cells (*esg*^{ts}>+), Myospheroid (Mys)–a β-subunit of *Drosophila* integrin–signals were detected at the basal and the lateral sides of the cells (Fig. 3.3C). Similarly, most *yki*$^{3S/A}$ cells that were not forming protrusions showed Mys signals at the basal and the lateral sides with signals that were stronger than those in control cells (Fig. 3.3C'). Intriguingly, in *yki*$^{3S/A}$ cells forming protrusions, Mys signals disappeared from the basal and the lateral sides of the cell body and accumulated at the protrusions (Fig. 3.3C'', arrows, cell body; arrowheads, protrusion). We also assessed the subcellular distribution of Multiple edematous wings (Mew)–an α-subunit of *Drosophila* integrin. Mew signals were not readily detectable in control *esg*$^{+}$ cells, probably due to low expression levels (Fig. 3.3D). In contrast, Mew signals were clearly visible at the basal and lateral sides in most *yki*$^{3S/A}$ cells, indicating that expression of *yki*$^{3S/A}$ increased Mew (Fig. 3.3D'). Notably, in *yki*$^{3S/A}$ cells forming protrusions, Mew signals were detected mainly at the protrusions (Fig. 3.3D'', arrows, cell body; arrowheads, protrusion). Additionally, wechecked the subcellular localization of Talin—a cytoplasmic protein that links integrins to the actin cytoskeleton. In control *esg*$^{+}$ and most of the *yki*$^{3S/A}$ cells, Talin signals were predominantly detected at the lateral and the basal sides (Fig. 3.3B and B'). In contrast, in *yki*$^{3S/A}$ cells forming protrusions, strong Talin signals were observed at the protrusions but were negligible in the cell bodies (Fig. 3.3B'', arrows, cell body; arrowheads, protrusion).

Taken together, these results show that only a portion of *yki*$^{3S/A}$ cells can produce large protrusions across the VM that are enriched for focal adhesion components, again suggesting that only a subpopulation of *yki*$^{3S/A}$ cells are migratory. The strong presence of Arm at cell-cell junctions of *yki*$^{3S/A}$ cells indicates that most *yki*$^{3S/A}$ cells are not migratory (Fig. 3.1A). Considering the assembly of focal adhesion components at the protrusions of *yki*$^{3S/A}$ cells, these protrusions might serve as attachments for pulling the cell bodies across the VM for cell dissemination.

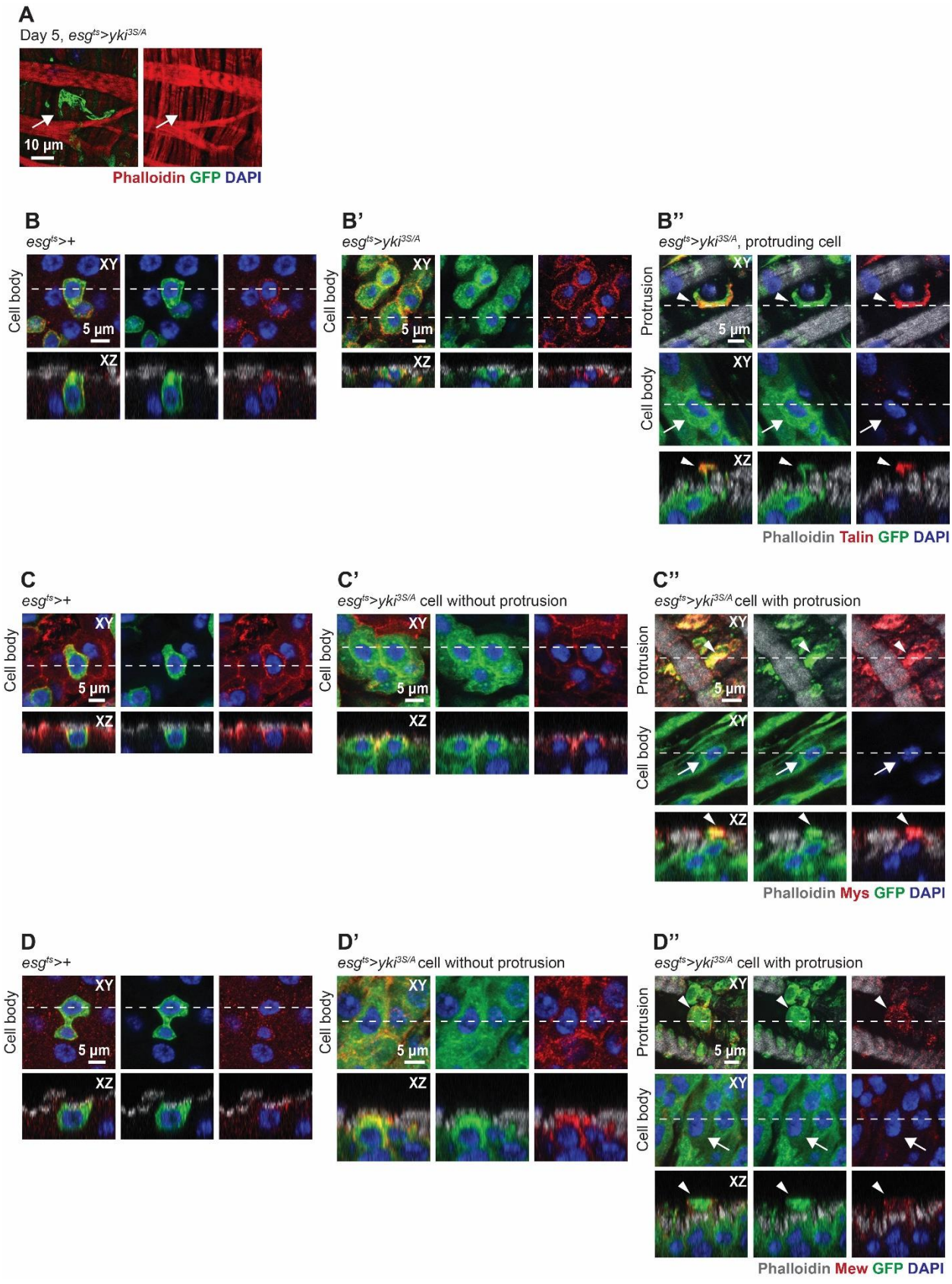
A
Day 5, esg^ts>yki^3S/A
10 µm
Phalloidin GFP DAPI
B
esg^ts>+
B'
esg^ts>yki^3S/A
B''
esg^ts>yki^3S/A, protruding cell
Cell body
Protrusion
XY
XZ
5 µm
Phalloidin Talin GFP DAPI
C
esg^ts>+
C'
esg^ts>yki^3S/A cell without protrusion
C''
esg^ts>yki^3S/A cell with protrusion
Phalloidin Mys GFP DAPI
D
esg^ts>+
D'
esg^ts>yki^3S/A cell without protrusion
D''
esg^ts>yki^3S/A cell with protrusion
Phalloidin Mew GFP DAPI

Figure 3.3. Focal adhesion components are upregulated in *yki$^{3S/A}$* cells and accumulated at the protruding leading edges.

A. Representative image of a protrusion generated from *yki$^{3S/A}$* cell. Phalloidin signals show the visceral muscle. *yki$^{3S/A}$* cells generate protrusions across the visceral muscle without damaging the tissue. **B-B''.** Talin localization in *esg^{+}* cell in control (*esg^{ts}*>+) and *esg^{ts}>yki$^{3S/A}$* midguts. Representative images of control cells (**B**), *yki$^{3S/A}$* cells without forming protrusions (**B'**), and *yki$^{3S/A}$* cell forming protrusions (**B''**) are shown. Phalloidin (gray) marks the visceral muscle. "Cell body panel" shows a z-stack spanning nuclei of *GFP^{+}* cells. "Protrusion panel" shows a view from outside. Arrowhead indicates a protrusion and arrow shows the corresponding cell body. **C-C''.** Cellular localization of Mys (red) in representative *esg^{ts}* cell (**C**), *yki$^{3S/A}$* cell without protrusion (**C'**), and *yki$^{3S/A}$* cell with protrusion (**C''**). Arrowhead is used to indicate protrusion observed at the surface of the visceral muscle. Arrow is used to indicate the body of *yki$^{3S/A}$* cell generating protrusion. **D-D''.** Cellular localization of Mew (red) in representative *esg^{ts}* cell (**D**), *yki$^{3S/A}$* cell without protrusion (**D'**), and *yki$^{3S/A}$* cell with protrusion (**D''**). Arrowhead is used to indicate protrusion observed at the surface of the visceral muscle. Arrow is used to indicate the body of *yki$^{3S/A}$* cell generating a protrusion.

Chapter 4: Arresting *yki*$^{3S/A}$ tumor cells in stem cell-like cells halts cell dissemination and abrogates JNK activation and Mmp1 expression in *yki*$^{3S/A}$ cells

Given the accumulation of differentiating EB-like cells in *yki*$^{3S/A}$ tumors, we decided to test the role of the EC differentiation program in dissemination of *yki*$^{3S/A}$ cells. Notch signaling triggers the generation of EBs and the subsequent differentiation of EBs into ECs (Micchelli & Perrimon, 2006). If *yki*$^{3S/A}$ cells use the same mechanism to generate the EB-like cells, inhibition of Notch signaling should significantly impact their differentiation process, which may result in an accumulation of ISC-like *yki*$^{3S/A}$ cells. Thus, we expressed dominant-negative Notch (*N*^{DN}) in *yki*$^{3S/A}$ cells and then assessed the nuclear size distribution to gain insights into the changes in *yki*$^{3S/A}$ cell populations. We found that *yki*$^{3S/A}$, *N*^{DN} tumors grew as big as *yki*$^{3S/A}$ tumors at day 8 of transgene induction (Fig. 4A). However, expression of *N*^{DN} in *yki*$^{3S/A}$ cells resulted in a reduction in the large-nucleated cell population (Fig. 4B' and C). Most of the extremely large nuclei disappeared when *N*^{DN} and *yki*$^{3S/A}$ were expressed together with *esg*^{ts} (Fig. 4B' and C). Thus, *yki*$^{3S/A}$, *N*^{DN} cells appeared to be more homogeneous than *yki*$^{3S/A}$ cells, were uniformly expressing Dl marker (Fig. 4B-D), and lack of Su(H)GBE-lacZ marker (Fig. S5), indicating that inhibition of Notch signaling in *yki*$^{3S/A}$ cells efficiently blocked their differentiation and enriched the *Dl*$^{+}$ cell population in *yki*$^{3S/A}$ midgut tumor, confirming that expression of *N*^{DN} in *yki*$^{3S/A}$ cells arrest these *GFP*$^{+}$ tumor cells to become ISC-like *yki*$^{3S/A}$ cells (Fig. 4E). Of significance, expression of *N*^{DN} almost completely abolished dissemination of *yki*$^{3S/A}$ cells at day 8 of transgene expression (Fig. 4F). Since a subpopulation of *yki*$^{3S/A}$ cells showed the phenotypes associated with invasive cell behavior, we tested how blocking the generation of cells in the EC lineage affected Mmp1 expression and JNK signaling in *yki*$^{3S/A}$, *N*^{DN} tumors. As previously described, *puc-lacZ* and Mmp1 signals were detected in a portion of larger *yki*$^{3S/A}$ cells and most of ECs in *yki*$^{3S/A}$ midguts (Fig. 4G and H). In contrast, in *yki*$^{3S/A}$, *N*^{DN} midguts, *puc-lacZ* and Mmp1 signals disappeared from *yki*$^{3S/A}$, *N*^{DN} cells and were detected exclusively in ECs (*GFP*$^{-}$ cells) (Fig. 4G and H). Consistent to the lack of Mmp1 expression in *yki*$^{3S/A}$, *N*^{DN} cells, while the degradation of inner laminin layer beneath the visceral muscle did not get rescued in *yki*$^{3S/A}$, *N*^{DN} tumors, we found a continuous outer laminin layer on (Fig. 4I). Taken together, these results demonstrate that blocking the EC differentiation program in *yki*$^{3S/A}$ tumors is sufficient to attenuate the invasive behavior of *yki*$^{3S/A}$ cells.

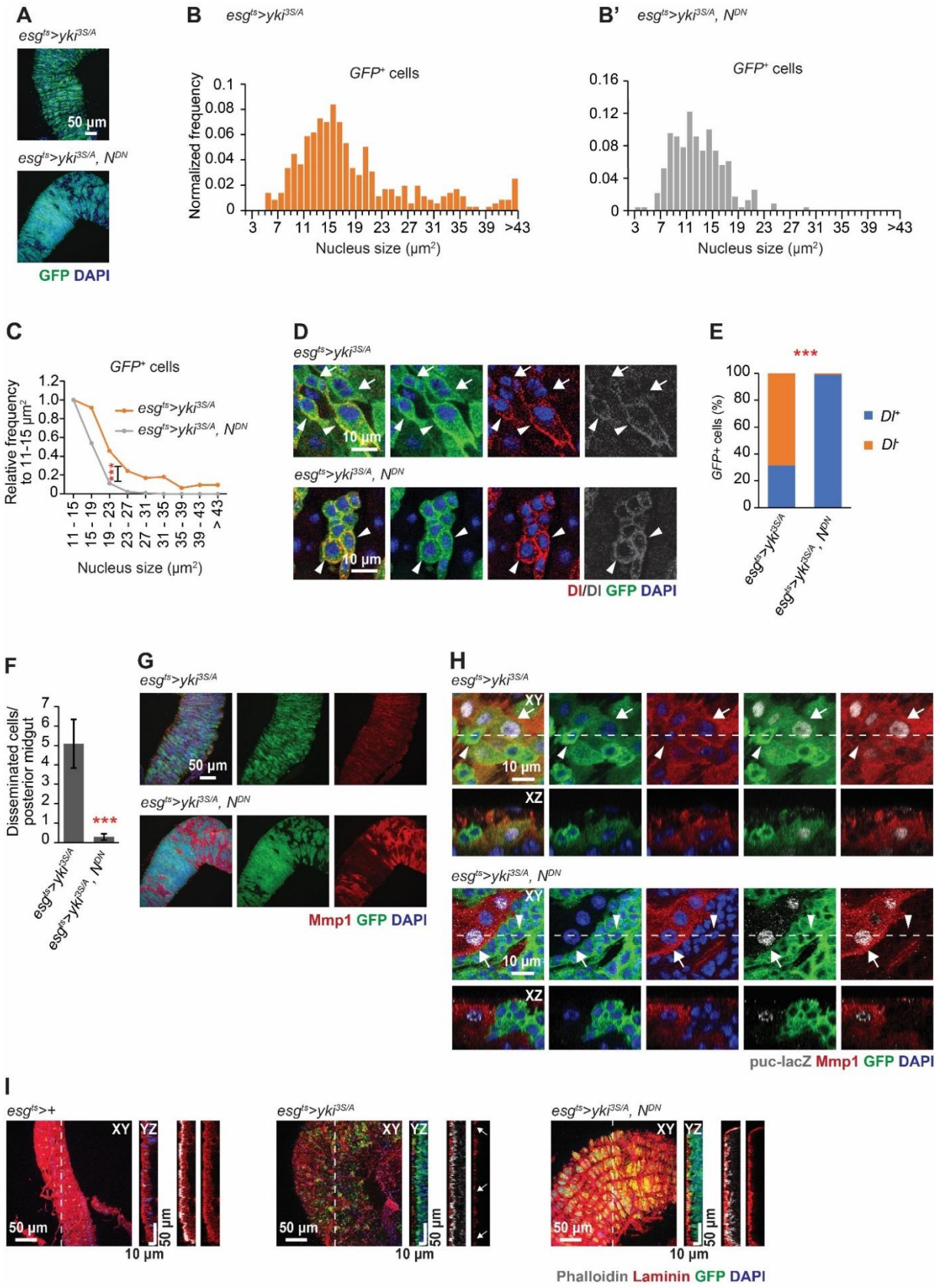
A
esg^ts>yki^3S/A
50 µm
esg^ts>yki^3S/A, N^DN
GFP DAPI
B
esg^ts>yki^3S/A
GFP+ cells
Normalized frequency
0.1
0.08
0.06
0.04
0.02
0
3 7 11 15 19 23 27 31 35 39 >43
Nucleus size (µm²)
B'
esg^ts>yki^3S/A, N^DN
GFP+ cells
0.16
0.12
0.08
0.04
0
3 7 11 15 19 23 27 31 35 39 >43
Nucleus size (µm²)
C
GFP+ cells
Relative frequency to 11-15 µm²
1.2
1.0
0.8
0.6
0.4
0.2
0
esg^ts>yki^3S/A
esg^ts>yki^3S/A, N^DN
11 - 15
15 - 19
19 - 23
23 - 27
27 - 31
31 - 35
35 - 39
39 - 43
> 43
Nucleus size (µm²)
D
esg^ts>yki^3S/A
10 µm
esg^ts>yki^3S/A, N^DN
10 µm
Dl/Dl GFP DAPI
E
***
GFP+ cells (%)
100
80
60
40
20
0
Dl+
Dl-
esg^ts>yki^3S/A
esg^ts>yki^3S/A, N^DN
F
Disseminated cells/ posterior midgut
7
6
5
4
3
2
1
0
***
esg^ts>yki^3S/A
esg^ts>yki^3S/A, N^DN
G
esg^ts>yki^3S/A
50 µm
esg^ts>yki^3S/A, N^DN
Mmp1 GFP DAPI
H
esg^ts>yki^3S/A
XY
10 µm
XZ
esg^ts>yki^3S/A, N^DN
XY
10 µm
XZ
puc-lacZ Mmp1 GFP DAPI
I
esg^ts>+
XY
YZ
50 µm
50 µm
10 µm
esg^ts>yki^3S/A
XY
YZ
50 µm
50 µm
10 µm
esg^ts>yki^3S/A, N^DN
XY
YZ
50 µm
50 µm
10 µm
Phalloidin Laminin GFP DAPI

Figure 4. Expression of N^{DN} in $yki^{3S/A}$ cells results in the accumulation of ISC-like $yki^{3S/A}$ cells, suppression of Mmp1 expression in $yki^{3S/A}$ cells and cell dissemination.

A. Representative images of $esg^{ts}>yki^{3S/A}$ and $esg^{ts}>yki^{3S/A}, N^{DN}$ midgut tumors. Transgenes were induced for 8 days. Tumor cells are marked by GFP (green). **B-B'.** Nucleus size distribution of GFP^{+} cells in $esg^{ts}>yki^{3S/A}$ midgut (**B**) and $esg^{ts}>yki^{3S/A}, N^{DN}$ midgut (**B'**) at day 6. **C.** Normalized Nuclear size distribution. Nucleus size distribution data shown in (**B and B'**) were binned by 4 μm starting from 11 μm, and then the binned values were normalized to the value from 11-15 μm^2 in each genotype. N=303 ($esg^{ts}>yki^{3S/A}$) and N=150 ($esg^{ts}>yki^{3S/A}, N^{DN}$) data points were analyzed. ***P<0.001, Chi-Square test. **D.** Representative images of GFP^{+} cells. Dl signals are shown in red and gray, and $yki^{3S/A}$ and $yki^{3S/A}, N^{DN}$ cells are marked by GFP (green). Transgenes were induced for 6 days. Arrow indicates representative GFP^{+} cells without Dl signals and arrowhead points to representative GFP^{+} cells with Dl signals. **E.** The graph shows the proportion of GFP+ cells with or without Dl signals in $yki^{3S/A}$ midgut vs. in $yki^{3S/A}, N^{DN}$ midgut. N=576 cells from 11 $esg^{ts}>yki^{3S/A}$ midguts and N=1049 cells from 7 $esg^{ts}>yki^{3S/A}, N^{DN}$ midgut. ***P<0.001, Chi-Square test. **F.** Quantification of disseminated cells. Transgenes were induced for 8 days. N=22 ($esg^{ts}>yki^{3S/A}$) and N=14 ($esg^{ts}>yki^{3S/A}, N^{DN}$) midguts. Mean±SEMs are shown. ***P<0.001, two-tailed unpaired Student's t-test. **G.** Mmp1 staining (red) of posterior midguts after 8 days of transgene induction. **H.** Mmp1 and *puc-lacZ* co-staining of posterior midgut cells. Mmp1 signals are shown in red and *puc-lacZ* signals are shown in gray. Transgenes were induced for 6 days. Arrows show cells with Mmp1 signal and nuclear *puc-lacZ* signal, and arrowheads indicate cells lacking both Mmp1 and *puc-lacZ* signals. **I.** Laminin staining (red) of the midguts. Arrows indicate localized degradation of the laminin layer.

Chapter 5: Arresting *yki*$^{3S/A}$ tumor cells in stem cell-like cells alters the tumor's capacity to induce phenotypes associated with cachexia-like wasting

Tumors elicit various adverse effects on the host tissues and physiology in part by expressing secreted proteins (Argilés et al., 2014; Baracos et al., 2018; Figueroa-Clarevega & Bilder, 2015; J. Kim et al., 2021; Kwon et al., 2015; Petruzzelli & Wagner, 2016; Porporato, 2016; Song et al., 2019; Yeom et al., 2021). *yki*$^{3S/A}$ midgut tumors express multiple secreted factors, which play key roles in inducing the phenotypes associated with cachexia-like wasting, such as organ degeneration, metabolic abnormalities, and reduced lifespan (J. Kim et al., 2021; Kwon et al., 2015; Song et al., 2019). Given the observation that blocking the EC differentiation program in *yki*$^{3S/A}$ tumors suppressed the phenotypes associated with invasiveness, we assessed how expression of *N*^{DN} in *yki*$^{3S/A}$ tumors altered the tumor's propensity to induce the non-tumor-autonomous or systemic phenotypes. Blocking the EC differentiation program in *yki*$^{3S/A}$ tumors significantly suppressed the 'bloating syndrome' phenotype—the manifestation of cachexia-like wasting—which is characterized by a bloated abdomen due to an increased circulating fluid (Fig. 5A, upper panels and B). Expression of *N*^{DN} also fully rescued ovary atrophy observed in flies harboring *yki*$^{3S/A}$ midgut tumors (Fig.5A, bottom panels and C). The adult visceral cavity is filled with amorphous fat body–the adipose tissue in *Drosophila*–, which makes the ventral side of the abdomen opaquely yellow-whiteish (Kwon et al., 2015). Since the fat body was significantly degenerated in flies bearing *yki*$^{3S/A}$ midgut tumors, the abdomen became translucent (Fig. 5A, middle panels). In contrast, the abdomen of flies bearing *yki*$^{3S/A}$, *N*^{DN} midgut tumors mostly remained opaque (Fig. 5A, middle panels), indicating that expression of *N*^{DN} in *yki*$^{3S/A}$ tumors suppressed fat body degeneration. These wasting phenotypes are associated with the expression of ImpL2, the secreted antagonist of *Drosophila* insulin-like peptides (Dilps) (Honegger et al., 2008; Kwon et al., 2015; Lee et al., 2021). ImpL2 expressed in *yki*$^{3S/A}$ tumors induced a systemic reduction in insulin/IGF signaling, resulting in hyperglycemia (Kwon et al., 2015). Of note, expression of *N*^{DN} in *yki*$^{3S/A}$ midgut tumors significantly rescued the hyperglycemia phenotype, which was assessed by measuring trehalose levels (Fig. 5D). However, expression of *N*^{DN} in *yki*$^{3S/A}$ midgut tumors did not alleviate all the phenotypes associated with cachexia-like wasting. We assessed muscle degeneration in tumor-bearing flies by measuring their climbing defects. Interestingly, expression of *N*^{DN}

in the tumors failed to rescue climbing defects associated with *yki*$^{3S/A}$ tumors (Fig. 5E). Moreover, blocking the EC differentiation program in *yki*$^{3S/A}$ midgut tumors further shortened the lifespan of the tumor-bearing flies (Fig. 5F and F'). These observations differentiate the roles of the ISC-like and the differentiating EB-like cells in inducing the phenotypes associated with cachexia-like wasting. Moreover, these data provided evidence that the differentiation program recapitulated in *yki*$^{3S/A}$ tumors plays a key role in shaping the tumor's capacity to induce various non-tumor-autonomous phenotypes.

Previous studies have identified several tumor-derived factors eliciting various non-tumor-autonomous phenotypes (Bilder et al., 2021; Figueroa-Clarevega & Bilder, 2015; J. Kim et al., 2021; Kwon et al., 2015; Liu et al., 2022; Lodge et al., 2021; Song et al., 2019; Yeom et al., 2021). Thus, we assessed the expression of various tumor-driven factors. Indeed, we found that blocking the EC differentiation program in *yki*$^{3S/A}$ midgut tumors significantly impacted the expression of several tumor-derived factors. Previous studies have shown that tumor-derived ImpL2 and epithermal growth factors (EGFs), such as PDGF- and VEGF-related factor 1 (Pvf1) are required for inducing the wasting phenotypes, including ovary atrophy, muscle degeneration, hyperglycemia, and bloating syndrome (Figueroa-Clarevega & Bilder, 2015; Kwon et al., 2015; Song et al., 2019; Yeom et al., 2021). Notably, mRNA levels of *ImpL2* and *Pvf1* were significantly reduced in *yki*$^{3S/A}$, *N*^{DN} tumors compared to *yki*$^{3S/A}$ tumors. An EGF ligand, *vein* (*vn*) was shown to function locally to support *yki*$^{3S/A}$ tumor growth (Song et al., 2019). *vn* mRNA levels were also reduced while tumor growth was not affected (Fig. 5G). Recently, J. Kim et al., (2021) showed that the *Drosophila* Interleukin-6 orthologs Unpaired 2 (Upd2) and Unpaired 3 (Upd3) derived from imaginal disc tumors caused an aberrant permeability of the blood-brain barrier (BBB), therefore exposing the brain to various circulating molecules in the blood and resulting in the significant reduction in the lifespan of the tumor-bearing flies (J. Kim et al., 2021). As the BBB was also shown to be compromised in the flies bearing *yki*$^{3S/A}$ midgut tumors (J. Kim et al., 2021), we tested the expression of all three *unpaired* genes. *upd1* mRNA levels were similar in both tumors while *upd2 and upd3* mRNA levels were significantly increased in *yki*$^{3S/A}$, *N*^{DN} tumors compared to *yki*$^{3S/A}$ tumors (Fig. 5G). Yoem et al., (2021) has reported that eye tumors induced by an active *yki* allele (*yki*^{S168A}) express a *Drosophila* homolog of the mammalian insulin-like 3 peptide (INSL3) Dilp8, which induces anorexia in flies (Yeom et al., 2021). However, *dilp8* mRNA levels were unaltered in *yki*$^{3S/A}$ midgut tumors compared

to control midguts (Fig. 5G), and expression of N^{DN} also did not significantly change d*ilp8* mRNA levels (Fig. 5G). Lodge et al. recently reported that Mmp1 secreted from imaginal disc tumors induces larval fat body degradation, larval muscle detachment, and is essential to cause ovary degeneration when transplanted in adult abdominal cavity (Lodge et al., 2021). In $yki^{3S/A}$ tumors, we found a substantial elevation in *Mmp1* mRNA level, consistent to the fat body degradation and ovary atrophy in tumor host. Of note, we observed mRNA level of *Mmp1* was significantly reduced in $yki^{3S/A}$, N^{DN} tumors (Fig. 5G). These results indicate that blocking the EC differentiation program in $yki^{3S/A}$ midgut tumors alters the expression of the tumor-derived factors, which are responsible for the adverse non-tumor-autonomous or systemic phenotypes.

Given the role of ImpL2 and Pvf1 in inducing various wasting phenotypes, the reduction in *ImpL2* and *Pvf1* expression might account for the suppression of bloating syndrome, ovary atrophy, fat body degeneration, and hyperglycemia in flies bearing $yki^{3S/A}$, N^{DN} tumors. A previous study showed that *ImpL2* depletion in $yki^{3S/A}$ tumors rescued the severity of bloating syndrome and hyperglycemia without affecting the tumor growth (Kwon et al., 2015). Consistently, depletion of *ImpL2* in $yki^{3S/A}$, N^{DN} tumors further suppressed bloating syndrome and hyperglycemia (Fig. S6), indicating that residual ImpL2 expression in $yki^{3S/A}$, N^{DN} tumors was responsible for the incomplete suppression of these phenotypes by the elimination of the $yki^{3S/A}$ cells in the EC lineage. Additionally, the elevated expression of *upd2* could be a factor responsible for the further shortening of the lifespan in flies bearing $yki^{3S/A}$, N^{DN} tumors as tumor derived Upd2 impairs the BBB. The significant increase in *upd2* mRNA expression in $yki^{3S/A}$, N^{DN} tumors suggests that Upd2 is expressed in ISC-like $yki^{3S/A}$ cells. Notably, depletion of *upd2* resulted in complete suppression in the development of $yki^{3S/A}$ tumor and $yki^{3S/A}$, N^{DN} tumor (Fig. S7), supporting that Upd2 is expressed in ISC-like $yki^{3S/A}$ cells. Previous reports have shown that Upd2 is expressed in EBs and ECs during tissue maintenance and regeneration (Jiang & Edgar, 2009; Zhai et al., 2015). These results suggest a role for the ISC-like $yki^{3S/A}$ cell-derived Upd2 in inducing tumor growth as well as non-tumor-autonomous phenotypes. Altogether, these findings suggest that tumor cell type-dependent expression of the tumor-derived factors could be the mechanism by which halting the EC differentiation program alters the tumor's capacity to induce non-tumor-autonomous phenotypes.

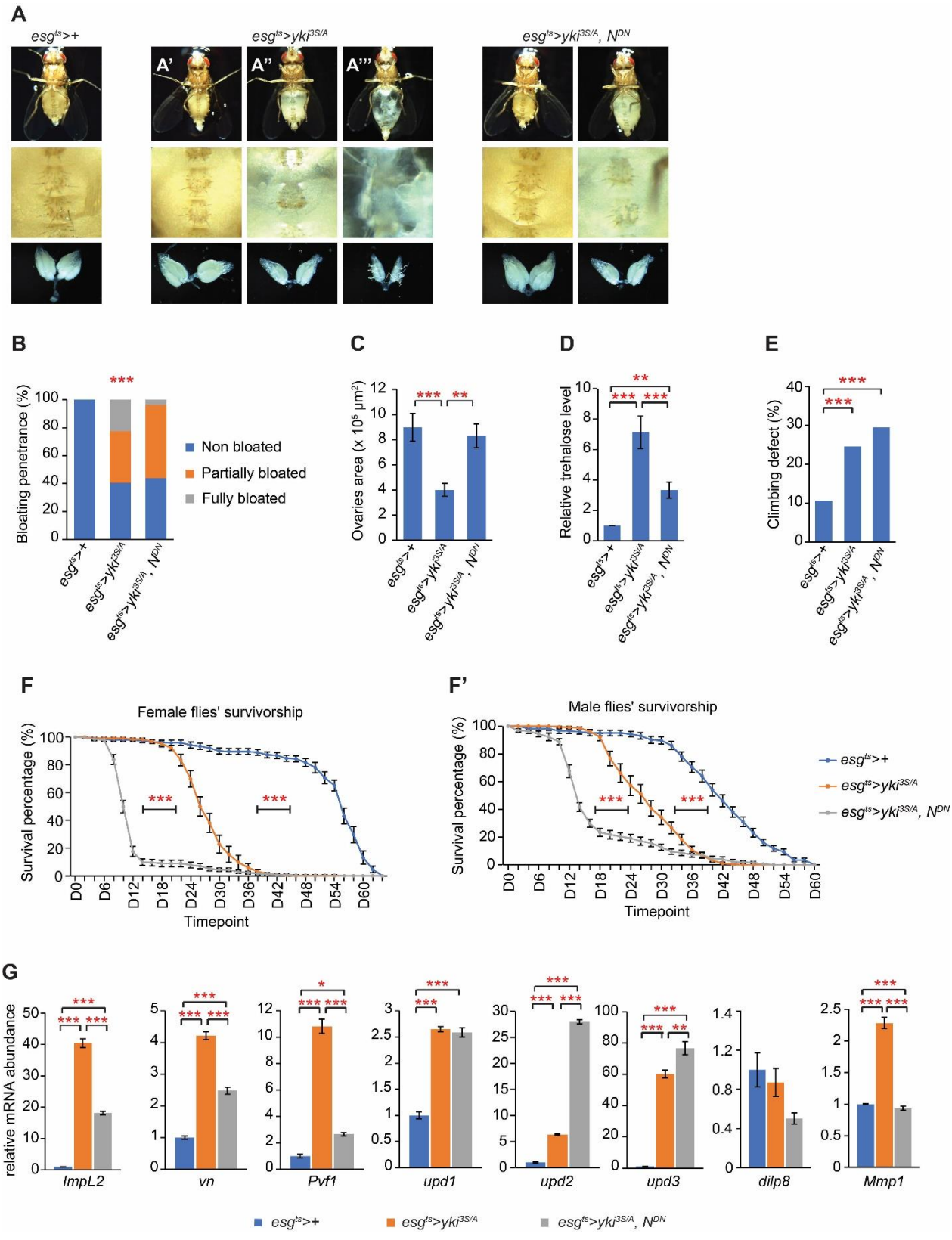
A
esg^ts>+
esg^ts>yki^3S/A
esg^ts>yki^3S/A, N^DN
A'
A''
A'''
B
Bloating penetrance (%)
Non bloated
Partially bloated
Fully bloated
C
Ovaries area (x 10^5 µm^2)
D
Relative trehalose level
E
Climbing defect (%)
F
Female flies' survivorship
Survival percentage (%)
Timepoint
F'
Male flies' survivorship
G
relative mRNA abundance
ImpL2
vn
Pvf1
upd1
upd2
upd3
dilp8
Mmp1

Figure 5. Blocking the EC differentiation program in *yki$^{3S/A}$* cells alters the phenotypes associated with cachexia-like wasting.

A. Representative ventral views and ovary images. Upper panels, ventral views; middle panels, magnified views of the corresponding fly's abdominal area; lower panels, images of the corresponding fly's ovaries. The upper panels in *esg^{ts}>yki$^{3S/A}$* show representative non-bloated (normal state) (**A'**), partially bloated (**A''**), and fully bloated (**A''**) fly's abdominal views. Transgenes were induced for 8 days. **B.** Quantification of bloating syndrome penetrance. Transgenes were induced for 8 days. Total N=481 (*esg^{ts}>+*), N=568 (*esg^{ts}>yki$^{3S/A}$*), and N=375 (*esg^{ts}>yki$^{3S/A}$, N^{DN}*) animals were pooled from 11 independent experiments. ***P<0.001, Chi-Square test (p<0.001) followed by Chi-Square pairwise comparison post-hoc test with Bonferroni Adjustment for Partially bloated and Fully bloated groups between *esg^{ts}>yki$^{3S/A}$* and *esg^{ts}>yki$^{3S/A}$, N^{DN}*. **C.** Quantification of ovaries size. Transgenes were induced for 8 days. N=19 (*esg^{ts}>+*), N=20 (*esg^{ts}>yki$^{3S/A}$*), and N=17 (*esg^{ts}>yki$^{3S/A}$, N^{DN}*) pairs of ovaries. Mean±SEMs are shown. **P<0.01, ***P<0.001, ANOVA test (p<0.001) followed by Tukey's post-hoc test. **D.** Relative trehalose levels in *esg^{ts}>+, esg^{ts}>yki$^{3S/A}$, and esg^{ts}>yki$^{3S/A}$, N^{DN}* flies at day 8 of transgene induction. Mean±SEMs are shown. N=6 flies, 6 biological replicates. **P<0.01, ***P<0.001, ANOVA test (p<0.001) followed by Tukey's post-hoc test. **E.** Representative quantification of climbing ability in *esg^{ts}>+*, *esg^{ts}>yki$^{3S/A}$*, and *esg^{ts}>yki$^{3S/A}$, N^{DN}* flies at day 14 of transgene induction. Total N=756 (*esg^{ts}>+*), N=848 (*esg^{ts}>yki$^{3S/A}$*), and N=250 (*esg^{ts}>yki$^{3S/A}$, N^{DN}*) were pooled from 19 independent experiments. ***P<0.001, Chi-Square (p<0.001) test followed by Chi-Square pairwise comparison post-hoc tests with Bonferroni Adjustment. **F-F'.** Survivorship of control flies vs. tumor bearing flies separated by gender. (**F**) The experiment in female flies was performed at 29°C to maintain the expression of transgenes. *esg^{ts}>+,* blue, N=159 flies in 17 replicates; *esg^{ts}>yki$^{3S/A}$*, orange, N=221 flies in 17 replicates; *esg^{ts}>yki$^{3S/A}$*, *N^{DN}*, gray, N= 224 flies in 18 replicates. Mean±SEMs are shown. ***p < 0.001, log-rank test. (**F'**) Survivorship in male flies, *esg^{ts}>+* intestine, blue, N=198 flies in 20 replicates; *esg^{ts}>yki$^{3S/A}$*, orange, N=203 flies in 18 replicates; *esg^{ts}>yki$^{3S/A}$*, *N^{DN}*, gray, N=210 flies in 20 replicates. Mean±SEMs are shown. ***p < 0.001, log-rank test. **G.** Relative mRNA levels of various wasting factors at day 8 of transgene induction. N=20 female midguts for each genotype, 3 biological replicates. Mean±SEMs are shown. *P<0.05, **P<0.01, ***p < 0.001, ANOVA test (p<0.001) followed by Tukey's post-hoc test.

Chapter 6: The role of EB-like *yki*$^{3S/A}$ tumor cells in shaping *yki*$^{3S/A}$ midgut tumor behaviors

6.1. Driving *yki*$^{3S/A}$ tumor cell differentiation to become EB-like cells also suppresses the invasive properties in *yki*$^{3S/A}$ cells

Given the accumulation of ISC-like cells in *yki*$^{3S/A}$ tumors (*yki*$^{3S/A}$, *N*^{DN} tumor cells, Chapter 4) resulted in the suppression of the invasive behavior of *yki*$^{3S/A}$ cells and the alteration in tumor's capacity to induce cachexia-like wasting phenotypes, we attempted to uncover the role of *yki*$^{3S/A}$ tumor cells in other cell state(s) in defining *yki*$^{3S/A}$ tumor behaviors. Expression of Zfh2 transcription factor in ISCs and newly differentiated EBs has been shown to be essential and sufficient to initiate EB differentiation towards EC and constitutive expression of Zfh2 prevents EBs to terminally differentiate into ECs (Rojas Villa et al., 2019). Considering that *yki*$^{3S/A}$ cells adopt the typical Notch-induced EC-differentiation to become heterogeneous cells (as discussed in Chapter 4), we hypothesized that Zfh2 might also play a consistent role in inducing *yki*$^{3S/A}$ cell differentiation, resulting in an accumulation of EB-like and differentiating EB-like *yki*$^{3S/A}$ cells. Hence, we expressed a wild-type allele of Zfh2 (*Zfh2*^{EAB}) in *yki*$^{3S/A}$ cells and evaluated its effect on *yki*$^{3S/A}$ cell populations using nuclear size distribution analysis. We found that *yki*$^{3S/A}$, *Zfh2*^{EAB} tumor develops at a quicker pace than *yki*$^{3S/A}$ tumor, reaching a fully grown tumor at day 4 post induction while *yki*$^{3S/A}$ tumor just began to become hyperplastic. (Fig. 6.1A). Expression of *Zfh2*^{EAB} in *yki*$^{3S/A}$ cells resulted in an accumulation of *GFP*$^{+}$ cells with nucleus >15 μm^2, especially those with extremely large nucleus population (Fig. 6.1B' and C). We also observed that the majority of *GFP*$^{+}$ cells were positive for Su(H)GBE-lacZ marker (Fig. 6.1D). Altogether, these data indicate that *Zfh2*^{EAB} expression in *yki*$^{3S/A}$ cells arrest these *GFP*$^{+}$ tumor cells in EB-like and differentiating EB-like *yki*$^{3S/A}$ cells. Unlike in *yki*$^{3S/A}$ tumors, most of the *GFP*$^{+}$ cells in *yki*$^{3S/A}$, *Zfh2*^{EAB} midgut tumors get eliminated from the intestinal epithelium by day 6 (Fig. 6.1A), suggesting a migratory behavior in these cells. Surprisingly, despite the robust protrusion formations through the visceral muscle layer, we did not observe basal cell dissemination in *yki*$^{3S/A}$, *Zfh2*^{EAB} tumors. Instead, we found *yki*$^{3S/A}$, *Zfh2*^{EAB} cells apically delaminated towards the midgut lumen, presumably explains the *GFP*$^{+}$ cell clearing phenomenon seen at day 6 (Fig. 6.1E). In previous chapters (Chapter 3 and 4), we illustrated our observations of Mmp1 expression in a portion of larger *yki*$^{3S/A}$ cells and most of ECs in *yki*$^{3S/A}$ midguts, but not in the ISC-like *yki*$^{3S/A}$ cells (Fig. 6.1F). However,

despite possessing larger cell morphology, *yki*$^{3S/A}$, *Zfh2*^{EAB} cells were lacking in Mmp1 signals (Fig. 6.1F). Expectedly, the absence of Mmp1 signal in *yki*$^{3S/A}$, *Zfh2*^{EAB} cells corresponded to the intact laminin layer in *yki*$^{3S/A}$, *Zfh2*^{EAB} tumors (Fig. 6.1G). Altogether, our observations demonstrate that enriching EB-like cells and differentiating EB-like cells in *yki*$^{3S/A}$ tumor also eliminates *yki*$^{3S/A}$ cell invasiveness.

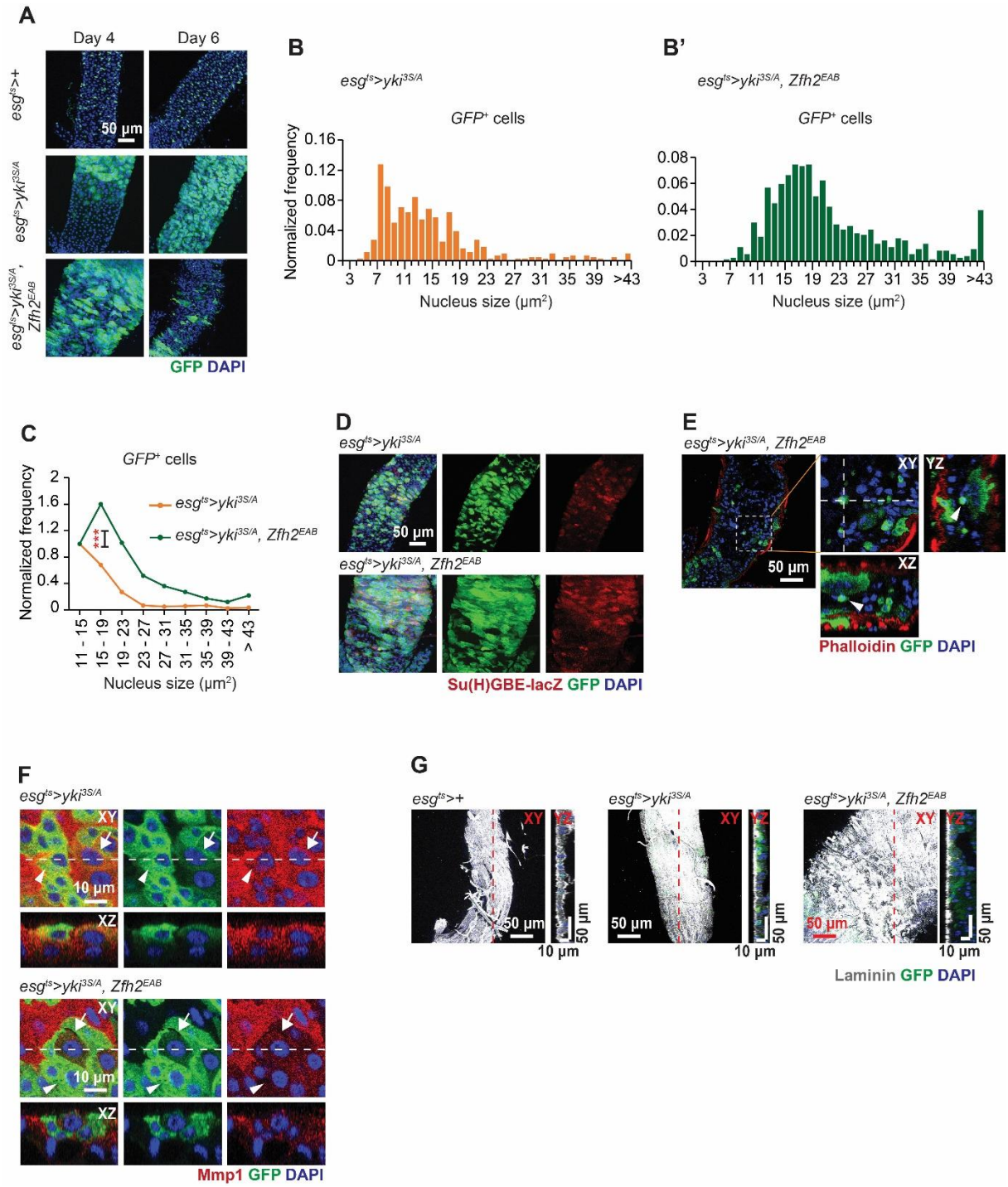

Figure 6.1. Arresting *yki$^{3S/A}$* tumor cells in EB-like cells also suppresses the invasive properties in *yki$^{3S/A}$* cells.
A. Representative images of *esg^{ts}*>+, *esg^{ts}>yki$^{3S/A}$* and *esg^{ts} >yki$^{3S/A}$, Zfh2^{EAB}* midgut tumors. Transgenes were induced for 4 and 6 days. Tumor cells are marked by GFP (green). **B-B'.** Nucleus size distribution of *GFP^{+}* cells in *esg^{ts}>yki$^{3S/A}$* midgut (**B**) and *esg^{ts} >yki$^{3S/A}$, Zfh2^{EAB}* midgut (**B'**) at day 4. **C.** Normalized Nuclear size distribution. Nucleus size distribution data shown in (**B and B'**) were binned by 4 μm starting from 11 μm, and then the binned values were normalized to the value from 11-15 μm^2 in each genotype. N=268 (*esg^{ts}>yki$^{3S/A}$*) and N=702 (*esg^{ts} >yki$^{3S/A}$, Zfh2^{EAB}*) data points were analyzed. ***P<0.001, Chi-Square test. **D.** Representative images of *esg^{ts}>yki$^{3S/A}$* and *esg^{ts} >yki$^{3S/A}$, Zfh2^{EAB}* midgut tumors. Su(H)GBE signals are shown in red, while *yki$^{3S/A}$* and *esg^{ts} >yki$^{3S/A}$, Zfh2^{EAB}* cells are marked by GFP (green). Transgenes were induced for 4 days. **E.** Representative image of the inside of *esg^{ts} >yki$^{3S/A}$, Zfh2^{EAB}* posterior midgut at day 6. Arrowhead points to apically delaminating *yki$^{3S/A}$, Zfh2^{EAB}* cells into lumen. **F.** Mmp1 staining (red) of posterior midguts after 4 days of transgene induction. **G.** Laminin staining (gray) of the midguts 4 days post transgene induction.

6.2. Enriching EB-like cells in *yki$^{3S/A}$* tumor enhances tumor's capacity to induce cachexia-like wasting phenotypes

Considering that preventing EB-like *yki$^{3S/A}$* cells from terminally differentiating into EC also abolished invasiveness-related properties, we evaluated *yki$^{3S/A}$, Zfh2^{EAB}* tumor's capacity to stimulate the phenotypes associated with cachexia-like wasting in tumor host. Typically, flies bearing *yki$^{3S/A}$* midgut tumors at day 4 would not yet develop bloating syndrome resulting in flat abdominal cavity filled with amorphous fat body and would still have a pair of normal sized ovaries, likely due to the minimal tumor formation in the midgut (Fig. 6.2A-C). However, consistent with the grown state of the tumor, expression of *Zfh2^{EAB}* in *yki$^{3S/A}$* cells induced an earlier manifestation of more severe bloating syndrome phenotype, fat body degradation, and ovary atrophy at day 4 post transgenes inductions (Fig. 6.2A-C). Given the manifestation of these aggravated cachexia symptoms in *yki$^{3S/A}$, Zfh2^{EAB}* tumor flies, we evaluated the expression of tumor derived wasting factors. As expected, we found that enriching differentiating EB-like cells in *yki$^{3S/A}$* tumor significantly elevated the expression of these tumor-derived factors (Fig. 6.2D). In particular, the elevation in *ImpL2*, *Pvf1*, and *Mmp1* expression might explain the worsening symptoms of bloating syndrome, fat body degeneration, and ovary atrophy in flies bearing *yki$^{3S/A}$, Zfh2^{EAB}* tumors. Our findings show that accumulation of differentiating EB-like *yki$^{3S/A}$* cells resulted in an overall increase in wasting ligand expression profile, which exacerbated the severity of cachexia-like wasting phenotypes. Taken together, these data provided evidence to support that each distinct tumor cell state plays a unique

role in determining tumor's capacity to induce various non-tumor-autonomous phenotypes. Hence, the heterogeneous cell composition within tumors defines the overall tumor behaviors, including cachectic distant tissue wasting.

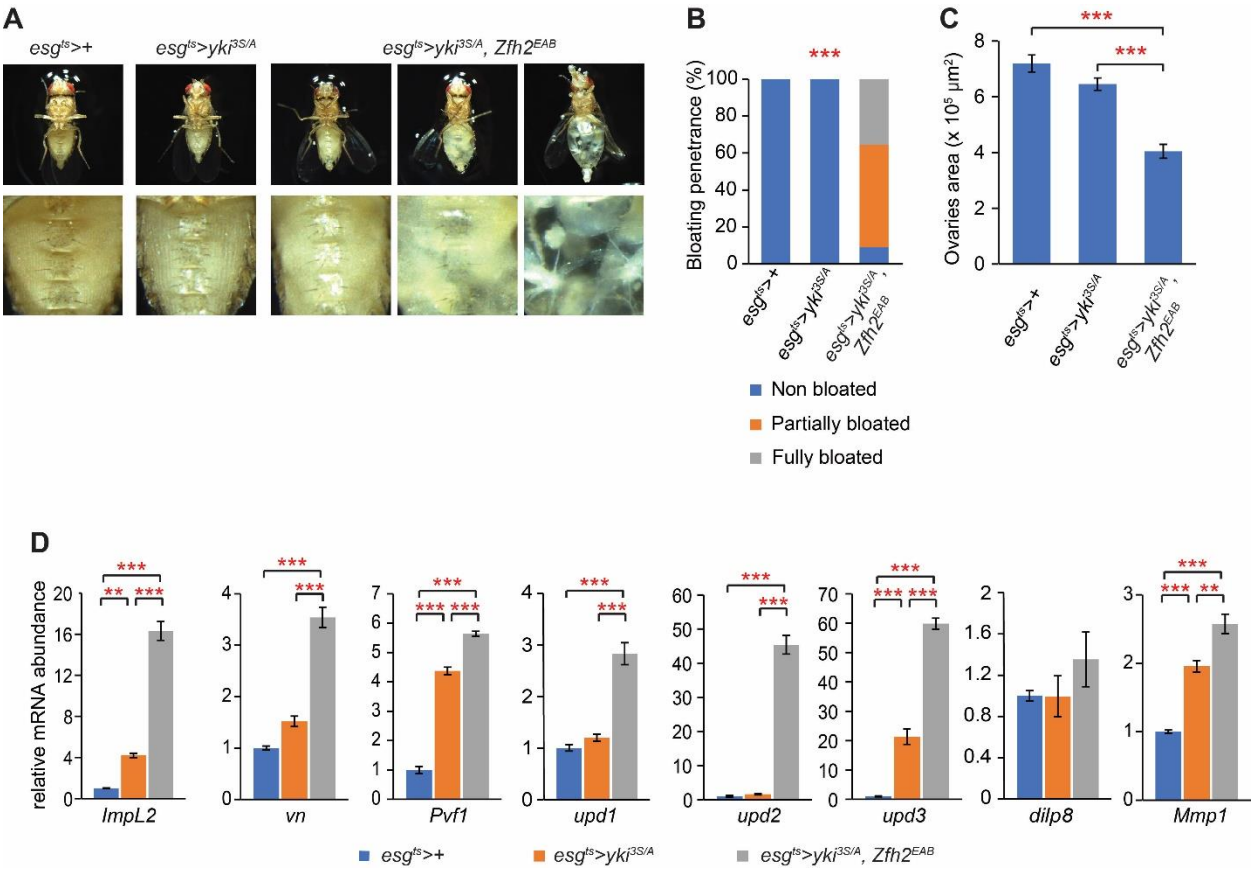

Figure 6.2. Arresting *yki$^{3S/A}$* tumor cells in EB-like cells aggravates cachexia-like wasting phenotypes in tumor host.

A. Representative abdominal ventral views. Upper panels, ventral views; lower panels, magnified views of the corresponding fly's abdominal area. The upper panels in *esg^{ts} >yki$^{3S/A}$, Zfh2^{EAB}* show representative non-bloated (normal state), partially bloated, and fully bloated fly's abdominal views, respectively from left to right. Transgenes were induced for 4 days. **B.** Quantification of bloating syndrome penetrance. Transgenes were induced for 4 days. Total N=309 (*esg^{ts}>+*), N=166 (*esg^{ts}>yki$^{3S/A}$*), and N=140 *esg^{ts} >yki$^{3S/A}$, Zfh2^{EAB}*) animals were pooled from 6 independent experiments. ***P<0.001, Chi-Square test (p<0.001) **C.** Quantification of ovaries size. Transgenes were induced for 4 days. N=43 (*esg^{ts}>+*), N=48 (*esg^{ts}>yki$^{3S/A}$*), and N=47 (*esg^{ts} >yki$^{3S/A}$, Zfh2^{EAB}*) pairs of ovaries. Mean±SEMs are shown. ***P<0.001, ANOVA test (p<0.001) followed by Tukey's post-hoc test. **D.** Relative mRNA levels of various wasting factors at day 4 of transgene induction. N=20 female midguts for each genotype, 3 biological replicates. Mean±SEMs are shown. *P<0.05, **P<0.01, ***p < 0.001, ANOVA test (p<0.001) followed by Tukey's post-hoc test.

Chapter 7: A discussion on the role of innate cell differentiation in generating tumor cell heterogeneity and its consequence on aggressive tumor behaviors

We demonstrate that the EC differentiation program is aberrantly recapitulated in *yki*$^{3S/A}$ midgut tumors, resulting in the generation of heterogeneous types of *yki*$^{3S/A}$ cells. Based on the markers of ISCs and EBs, Dl and Su(H)GBE-lacZ, respectively, *yki*$^{3S/A}$ cells could be divided into at least 3 different types: ISC-like (*Dl*$^{+}$), EB-like (*Su(H)GBE*$^{+}$), and ISC/EB-like (*Dl*$^{+}$, *Su(H)GBE*$^{+}$) (Fig. 2.2B-F). Although *Dl*$^{+}$, *Su(H)GBE*$^{+}$ cells were rarely detected in control midguts, a portion of *yki*$^{3S/A}$ cells were *Dl*$^{+}$, *Su(H)GBE*$^{+}$ (Fig. 2.2F). We observed an accumulation of *yki*$^{3S/A}$ cells with large nuclei, which were reminiscent of EBs undergoing differentiation into ECs (Fig. 2.2B' and D). The EC cell marker Pdm1 was occasionally detected in large *Su(H)GBE*$^{+}$ cells with reduced GFP signals. Thus, at least some *yki*$^{3S/A}$ cells appeared to undergo terminal differentiation to generate ECs (Fig. 2.2G). Interestingly, some nuclei of *yki*$^{3S/A}$ cells were even larger than the nuclei of normal EC cells, suggesting that a portion of *yki*$^{3S/A}$ cells deviate from the normal EC lineage (Fig. 2.2B). In this study, we presumed that the increasing nuclear size is positively correlated to the increasing nuclear contents and polyploidy as seen in the normal physiological context. However, since we did not directly investigate their nuclear contents, it is possible that some of these *yki*$^{3S/A}$ cells with extremely large nucleus might also be aneuploid. In the midgut epithelium, ISCs by default generate ISCs, and activation of Notch signaling triggers the EC lineage by generating EBs and initiating the differentiation of EBs into ECs (Boumard & Bardin, 2021; Hou & Singh, 2017; Jiang et al., 2016; Li & Jasper, 2016; Micchelli & Perrimon, 2006; Miguel-Aliaga et al., 2018; Ohlstein & Spradling, 2006). Of importance, inhibiting Notch signaling in *yki*$^{3S/A}$ tumors dramatically diminished the cellular heterogeneity by eliminating *yki*$^{3S/A}$ cells resembling the cells in the EC lineage, resulting in an accumulation of ISC-like *yki*$^{3S/A}$ cells (*Dl*$^{+}$). Altogether, our study reveals the heterogeneity of *yki*$^{3S/A}$ midgut tumor cells and elucidates the key role of the native EC differentiation program in generation of cellular heterogeneity.

Recent studies have revealed that the developmental and/or differentiation programs that form and maintain the tissues of origin are recapitulated in cancers, such as glioblastoma, Wilms tumors, and non-small-cell lung cancer (Couturier et al., 2020; Fukuzawa et al., 2017; Goveia et al., 2020; N. Kim et al., 2020; Wu et al., 2021; Yeo et al., 2020). However, it remains unclear how the developmental and

differentiation programs affect tumor progression and the tumor's capacity to induce various non-tumor-autonomous phenotypes, such as cachexia. Our findings provide us with an opportunity to use *Drosophila* genetics to discriminate the roles of ISC-like tumor cells and differentiating tumor cells in tumor progression as well as inducing the phenotypes associated with cachexia-like wasting. $yki^{3S/A}$ cells co-opting the EC differentiation program significantly accumulate, and inhibition of Notch signaling eliminates these differentiating $yki^{3S/A}$ cells, leading to a robust formation of tumors comprised of ISC-like $yki^{3S/A}$ cells. In contrast, accruing differentiating tumor cells in $yki^{3S/A}$ tumor through the expression of $Zfh2^{EAB}$ promotes rapid and advanced tumor formation. Interestingly, both eliminating and accumulating the differentiating tumor cells almost completely suppresses tumor cell basal dissemination and attenuates the phenotypes associated with invasive cell behavior. This implies either that (1) invasive $yki^{3S/A}$ tumor cells are abnormally differentiated tumor cells, or (2) dynamic cell states among tumor cells are essential during tumor progression for cell invasiveness. Thus, our study reveals an unexpected role of the differentiating tumor cells in the invasion process. It has been shown that Esg is expressed more in the EBs committed to differentiation than ISCs (Antonello, Reiff, Ballesta-Illan, et al., 2015; Korzelius et al., 2014). The committed EBs acquire mesenchymal characteristics, such as polarized shape and invasive properties (Antonello, Reiff, Ballesta-Illan, et al., 2015). This raises an interesting possibility that the intrinsically invasive properties of the EBs undergoing differentiation could be the origin of the invasiveness of $yki^{3S/A}$ cells. We speculate that the accumulation of $yki^{3S/A}$ cells resembling the intrinsically invasive EB pool might result in cell dissemination. Coordination of cell differentiation and migration is a wide-spread phenomenon in the development and tissue maintenance (Aalto et al., 2021; Antonello, Reiff, Ballesta-Illan, et al., 2015; Arvidsson et al., 2002; Montell, 2003; Parent et al., 2002; Peercy & Starz-Gaiano, 2020; Vasilyev et al., 2009). Therefore, we propose that an accumulation of aberrantly differentiating tumor cells induced by the developmental and differentiation programs could be a mechanism by which tumors acquire invasiveness.

Our study elucidates the differential roles of ISC-like and differentiating tumor cells in inducing the phenotypes associated with cachexia-like wasting. Depletion of the differentiating tumor cells by expressing N^{DN} significantly rescues an array of the phenotypes associated with cachexia-like wasting: ovary atrophy, fat body degeneration, hyperglycemia, and bloating syndrome. However, blocking cell

differentiation does not rescue muscle degeneration and further shortens the lifespan. Meanwhile, accumulation of differentiating tumor cells by expressing Zfh2^{EAB} significantly aggravates ovary atrophy, fat body degeneration, and bloating syndrome. These observations demonstrate the distinct roles ISC-like and differentiating tumor cells play in shaping the tumor's capacity to induce various non-tumor-autonomous phenotypes. Changing the tumor-cell population by blocking or promoting cell differentiation causes significant alterations in the expression of the tumor-derived wasting factors. Depletion of the differentiating tumor cells greatly reduces *ImpL2* mRNA expression in the tumors, and depletion of *ImpL2* in *yki*$^{3S/A}$, *N*^{DN} tumors further suppressed hyperglycemia and bloating syndrome. Meanwhile, accumulation of differentiating tumor cells increases the *ImpL2* mRNA expression in the tumors, corresponding to the advanced bloating syndrome and ovary atrophy observed in *yki*$^{3S/A}$, *Zfh2*^{EAB} tumors. These observations indicate that *ImpL2* is predominantly expressed in the differentiating tumor cells. In contrast, depletion of the differentiating tumor cells significantly increases *upd2* mRNA levels, and depletion of *upd2* in *yki*$^{3S/A}$, *N*^{DN} cells significantly suppressed tumor growth, indicating that Upd2 is primarily expressed in ISC-like tumor cells. Given the role of Upd2 in impairing the normal BBB function, the increase in Upd2 expression in *yki*$^{3S/A}$, *N*^{DN} tumors could account for the reduction in the lifespan of the tumor-bearing flies (J. Kim et al., 2021). However, it is important to note that other tumor-growth-related factors, such as a compromised intestinal barrier, the lack of nutrient-adsorptive capacity, and intestinal lumen blockage, may also contribute to the lifespan shortening observed in *yki*$^{3S/A}$, *N*^{DN} tumor-bearing flies. Thus, these observations indicate that these tumor-derived factors are differentially expressed in the ISC-like cells versus the differentiating-like tumor cells, which could be the basis for the alteration of non-tumor autonomous phenotypes upon reducing cellular heterogeneity. Altogether, these results show that tumor cell heterogeneity is a key factor that shapes the tumor's capacity to induce various non-tumor-autonomous and systemic phenotypes. Furthermore, our study provides mechanistic insight into how eliminating a tumor cell population can alter the tumor's capacity to induce non-tumor-autonomous phenotypes.

Simple genetic manipulations, such as the expression of an oncogene and the depletion of a tumor suppressor, induce hyperplasia in various tissues in *Drosophila*. These hyperplasias have been used as so-called *Drosophila* "tumor" models, which has led to the discovery of various fundamental

mechanisms underlying the growth of normal tissues as well as cancers (Bilder et al., 2021; Dong et al., 2007, 2021; Liu et al., 2022; Villegas, 2019; Yeom et al., 2021) Notably, *Drosophila* tumors can also induce various phenotypes reminiscent of those observed in advanced cancer patients. Since hyperplasias are normally induced within a few days, it is unlikely that these tumors acquire additional genetic alterations, which can confer new properties to the tumors. Therefore, the ability of tumors to induce certain phenotypes cannot be entirely dependent on the gain of an oncogene or loss of a tumor suppressor. Our study provides insights into how the native cell differentiation program can contribute to the tumor's capacity to induce various phenotypes. Moreover, our study raises the possibility of manipulating the advanced cancer phenotypes by altering the developmental and differentiation programs co-opted in tumors. Thus, it would be of interest to address how the developmental and differentiation programs recapitulated in cancers contribute to the induction of complications associated with cancers; a process in which might be manipulated in strategizing for finding more effective cancer cachexia treatments. Due to the lack in understanding and standardized cure for cancer cachexia, a common approach for the syndrome focuses on reversing the symptoms, such as by stimulating patients' appetite. Given that each tumor cell type expresses distinct cachexia factors into the circulation, the overall tumor cell composition would define cancer cachexia symptoms in a patient-specific manner. Hence, if we could halt the innate cell differentiation program to homogenize these tumor cells, perhaps we could more effectively target these homogenized tumor cells for elimination before they could induce cancer cachexia. Considering the plethora of knowledge on tissue development and the well-defined genetic tools for manipulating specific cell lineages, *Drosophila* tumor models provide an opportunity to further elucidate the underlying principles. It would be interesting to study how specific steps in cell differentiation are linked to specific tumor phenotypes and how different oncogenes interact with the native developmental and differentiation programs to impact tumor cell heterogeneity and give rise to different non-tumor-autonomous and systemic phenotypes.

Chapter 8: Methods

8.1. Fly genetics and husbandry

Fly crosses were maintained in vials with standard cornmeal-agar medium and kept at 18°C throughout development and adulthood until ready for temperature-dependent induction. For all experiments, except for climbing and lifespan assays, zero to three-day-old female flies were collected and were shifted to 29°C to induce transgene expression for the indicated number of days prior to dissection. During the 29°C incubation, flies were transferred to fresh food vials every 2 days. To manipulate ISCs and EBs, we used *esg-GAL4, tub-GAL80^{ts}, UAS-GFP* (referred to as *esg^{ts}*). Fly strains used in this study included: *UAS-yki$^{3S/A}$* (*w**;; *UAS-yki.S111A.S168A.S250A.V5*) (BDSC #28817), *UAS-yki^{S168A}* (BDSC #28818), *Su(H)GBE-lacZ* (BDSC #83352), *UAS-Mmp1 RNAi* JF01136 (BDSC #31489), *UAS-ImpL2 RNAi* HMC05809 (BDSC #64936), *UAS-upd2 RNAi* HMS00901 (BDSC #33949), *UAS-upd2 RNAi* HMS00948 (BDSC #33988), *UAS-Zfh2^{EAB}* (BDSC #56545), *puc-lacZ* (laboratory stock), *UAS-Notch^{DN}* (laboratory stock).

8.2. Antibodies and immunofluorescence imaging

Immunostainings performed in this study used the following primary antibodies: anti-GFP antibody, Alexa Fluor® 488 (1:1000; Thermo Fisher Scientific, A-21311; rabbit), anti-Armadillo antibody (1:1000; DSHB, N2 7A1; mouse), anti-laminin B1 antibody (1:1000; Abcam, ab47650; rabbit), anti-Mmp1 antibody (1:100; DSHB, 3B8D12; mouse), anti-Mys antibody (1:1000; DSHB, CF.6G11; mouse), anti-Mew antibody (1:300; DSHB, DK.1A4; mouse), anti-Talin antibody (1:1000; DSHB, A22A; mouse), anti-Delta antibody (1:1000; DSHB, C594.9B; mouse), anti-Pdm1 antibody (1:500; a gift from the Cai Lab; rabbit), anti-β Galactosidase antibody (1:1000; Cappel, 55976; rabbit and 1:1000; DSHB, 40-1a; mouse), anti-Prospero antibody (1:1000; DSHB, MR1A; mouse). All secondary antibodies were obtained from Thermo Fisher Scientific: anti-rabbit IgGs conjugated to Alexa Flour 594 (1:1000; A-11012; goat), anti-mouse IgGs conjugated to Alexa Flour 594 (1:1000; A-11005; goat), anti-rabbit IgGs conjugated to Alexa Flour 647 (1:1000; A-21244; goat), and anti-mouse IgGs conjugated to Alexa Flour 647 (1:1000; A-21235; goat). Filamentous actin was stained with phalloidin conjugated to Alexa Fluor 594 or 647 (1:1000; Thermo

Fisher Scientific, A-12381, A-22287, respectively). Nuclei were stained with DAPI (1:2000; Sigma-Aldrich, D9542).

To remove auto-fluorescing remnants from the midguts, we fed flies 4% sucrose for ~4 hr prior to dissection. Midgut samples were dissected in PBS, fixed in 4% paraformaldehyde (PFA) (Electron Microscopy Sciences, RT15710) diluted in PBS for 20 min, and then washed three times with PBST (PBS supplemented with 0.2% Triton X-100) with 5 min intervals. For permeabilization and blocking, we incubated tissue samples in blocking buffer (PBST supplemented with 5% normal goat serum) for 1 hr at room temperature. The tissue samples were incubated with primary antibodies in the blocking buffer overnight at 4°C. The samples were washed three times with PBST and then incubated in secondary antibodies for 2 hr at room temperature. Stained midguts were washed three times with PBST and preserved in Vectashield (Vector Laboratories, H-1000). Fluorescence images were acquired using a Leica SP8 laser scanning confocal microscope with 40×/1.25 oil objective lens. NIH ImageJ software was used for further adjustment and assembly of the acquired images.

8.3. Quantification of Armadillo signals

To measure the distribution and fluorescence intensity of Arm signals, we created a z-projection of a 50 µm × 50 µm region capturing the topmost epithelial leaflet from a 290.91 µm × 290.91 µm posterior midgut image. We drew a line from the outside of a cell across the cell body of all *GFP*$^{+}$ cells within the area. Mean gray values of the red channel (Arm signal) were collected using the Plot Profile function on NIH ImageJ software, giving a list of mean gray values at each distance point along the drawn line. These distance points were then adjusted to account for the line length differences among cells. Because Arm signals are predominantly at the membrane, the points where the line intersects the membrane would give the highest signal values. Out of the two distance points where the line intersects the membrane, the higher value was then used as 0 µm distance to calibrate the rest of the distance points, resulting in the distance points outside the cell as -X µm and distance points inside of the cells as +X µm. A total of four-50 µm × 50 µm-regions were created and analyzed for each intestine to cover the span of the posterior midgut.

8.4. Quantification of disseminated cells

Disseminated cells quantified in this study were defined as *GFP*$^{+}$ and *DAPI*$^{+}$ cells residing more basally than the visceral muscle (labeled with phalloidin) of the front epithelial leaflet. A series of z-stack images were taken to capture the posterior midguts using confocal microscopy. To determine cell positions respective to the visceral muscle layer, we reconstituted orthogonal views from the z-stacks images. The total number of disseminated cells was quantified in 290.91 µm × 290.91 µm confocal microscope fields.

8.5. Quantification of Mmp1 intensity

To measure the fluorescence intensity of Mmp1, we imaged the posterior midgut epithelium using confocal microscopy and generated z-projections using NIH ImageJ software. While only having the green channel on display, we collected measurements of mean gray values of the red channel (Mmp1 signal) using 2.84 µm × 2.84 µm fields for ten random *GFP*$^{+}$ cells and ten random polyploid, *GFP*$^{-}$ cells (ECs) per intestine along the span of the posterior midgut. The values were then subtracted by the background value, which was obtained by measuring the mean gray value of the outside area surrounding the tissue. All intensity values were normalized to the intensity value of *GFP*$^{+}$ cells in *esg*^{ts} intestine.

8.6. Nucleus size measurement analysis

To measure nucleus size, we created a z-projection of a 50 µm × 50 µm region capturing the topmost epithelial leaflet from a 290.91 µm × 290.91 µm posterior midgut image. We generated an RGB image of the DAPI channel (nuclei channel) only, made the image to an 8-bit type image, and converted them into a binary image. We applied a feature called Watershed to separate nuclear clusters due to cell crowding. The area of each nucleus was measured by subjecting the final binary image to Analyze Particles feature on NIH ImageJ software. All area measurements were filtered manually to exclude artifact quantifications by comparing the binary image to the original 50 µm × 50 µm RGB image. At least four-50 µm × 50 µm-regions were created and analyzed for each intestine to cover the span of the posterior midgut. The cell frequency data were normalized to the total number of quantified cells and displayed in histograms of 1 µm^2 bin increment with 43 µm^2 as the size cap. To show the relative abundance of cell populations within

the intestine in comparison to our arbitrary internal control (11-15 μm^2 bin), we binned our data into groups with 4 μm^2 bin increment and normalized the data to the cell frequency in the 11-15 μm^2 bin. We then displayed the relative values as line graphs.

8.7. Quantification of *Dl*$^+$, *GFP*$^+$ cells

To quantify the number of *GFP*$^+$ cells with or without Dl signals, we created a z-projection of a 50 µm × 50 µm region capturing the topmost epithelial leaflet from a 290.91 µm × 290.91 µm posterior midgut image. We scored *GFP*$^+$ cells with Dl signal on the membrane as *Dl*$^+$ cells. A total of four-50 µm × 50 µm-regions were created and analyzed for each intestine to cover the span of the posterior midgut.

8.8. Quantification of *Pros*$^+$ cells

To quantify the number of EE cells, we took a series of 290.91 µm × 290.91 µm z-stack images of posterior midgut region stained with anti-*Prospero* antibody. We created a z-projection of 100 µm × 100 µm field at the anterior-end of the top leaflet posterior midgut region and scored the *Pros*$^+$ cells.

8.9. Measurement of trehalose level

To prepare fly lysates for trehalose assays, we homogenized six female flies of each genotype in 400 µL PBST, heated the lysate at 70°C for 5 min, centrifuged the samples at 14,000 rpm for 10 min, and collected the supernatant. Whole-body trehalose levels were measured using a trehalose assay kit (Neogen; K-TREH) according to the manufacturer's protocol. The final value of trehalose levels was normalized to number of flies and then to trehalose level in control flies to obtain relative trehalose levels for each genotype.

8.10. Quantification of flies climbing ability assay

To assess climbing ability, we used flies at 14 days post induction. We transferred them into vials with a 2-cm mark from the food surface with a maximum capacity of 15 flies per vial. To record the climbing ability, we tapped down a vial five times to bring the flies to the bottom and recorded the number of flies that climbed to pass the 2-cm mark in 3 seconds. Flies with a climbing defect were defined as those that were not able to pass the mark in 3 seconds. Climbing ability assay was recorded 3 times for each vial.

All data from the same reading number across 19 independent experiments were pooled and analyzed together, resulting in 3 climbing ability graphs (reading #1, reading #2, and reading #3).

8.11. *Drosophila* lifespan assay

We collected adult female and male flies in separate vials with less than 25 individuals per vial and kept them at 29 °C incubator for transgenes induction. We transferred flies into fresh food vials and recorded deaths every two days.

8.12. Quantitative RT-PCR

We isolated total RNA from 20 adult female midguts or six female thoraces at D8 of induction with TRIzol (Invitrogen, Cat# 15596026). We used 1 µg of RNA to produce cDNA with iScript™ Reverse Transcription Supermix (Bio-Rad, Cat#1725120). The cDNA was subjected to quantitative real-time PCR with iTaq™ Universal SYBR Green Supermix (Bio-Rad, Cat#1708840) and CFX-96 (Bio-Rad). The fold-changes in RNA transcript levels were normalized against RpL32 gene, and further normalized to the control genotype for relative mRNA expression levels. Primer sequences are the following: *Pvf1*, CTGTCCGTGTCCGCTGAG, CTCGCCGGACACATCGTAG; *vn*, GAACGCAGAGGTCACGAAGA, GAGCGCACTATTAGCTCGGA; *dilp8*, GGACGGACGGGTTAACCATT, CATCAGGCAACAGACTCCGA; *ImpL2*, AAGAGCCGTGGACCTGGTA, TTGGTGAACTTGAGCCAGTCG; *upd1*, CCTACTCGTCCTGCTCCTTG, TGCGATAGTCGATCCAGTTG; *upd2*, CATCGTCATCCTCATCATCG, ATGTTCCGCAAGTTTTCGAG; *upd3*, AAATTCGACAAAGTCGCCTG, TTCCACTGGATTCCTGGTTC; *RP49*, GCTAAGCTGTCGCACAAATG, GTTCGATCCGTAACCGATGT.

8.13. Statistics and reproducibility

We performed two-tailed unpaired Student’s T-test statistical analyses using Microsoft Excel and ANOVA and post-hoc statistical analyses using IBM SPSS Statistics. Levels of significance are depicted by asterisks in the figures: *P<0.05, **P<0.01, ***P<0.001. Sample sizes were chosen empirically based on the observed effects and listed in the figure legends.

Supplemental figures

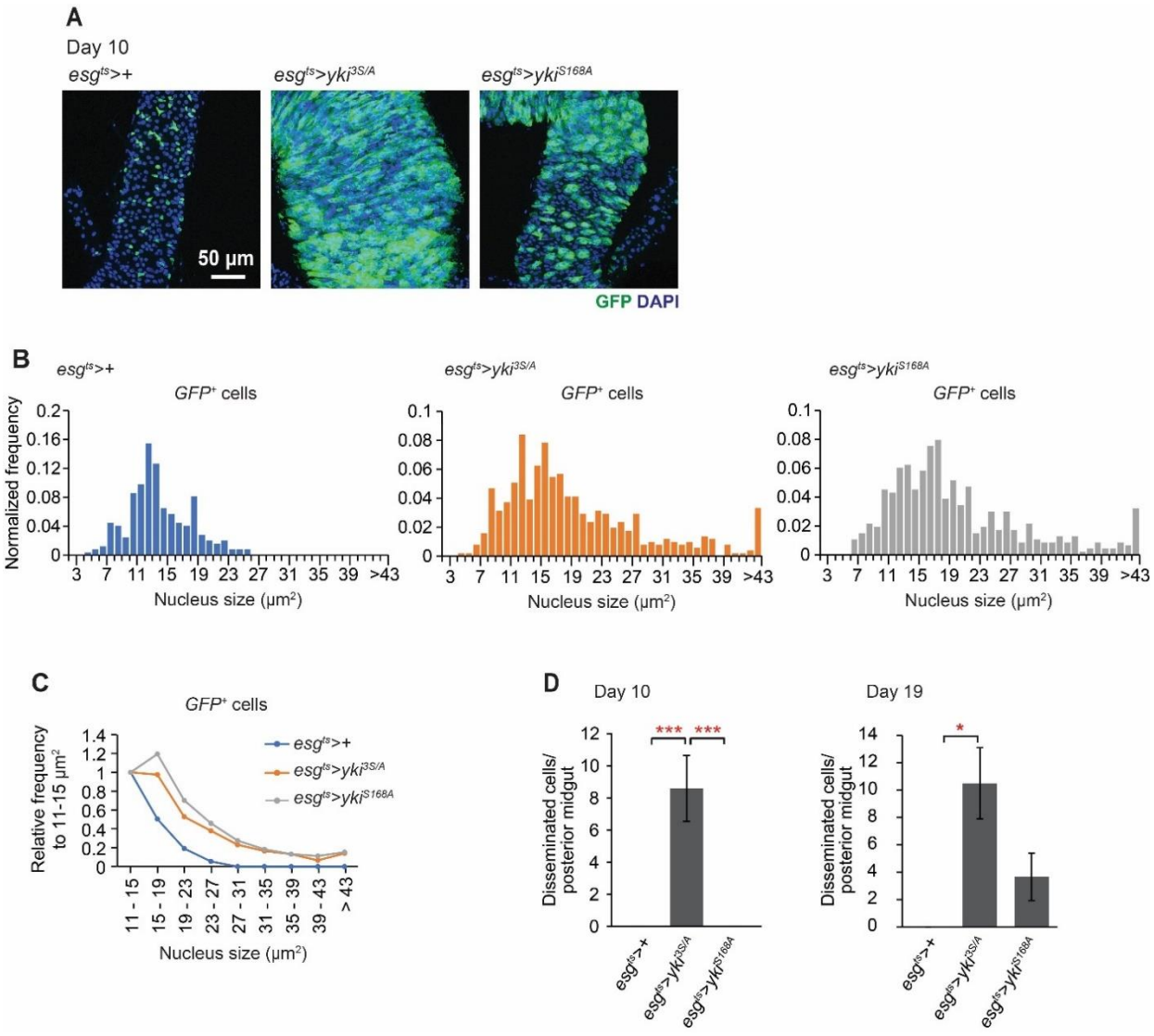

Figure S1. Characteristics comparison between *yki$^{3S/A}$* and *yki^{S168A}* hyperplastic midgut tumors. **A.** Posterior midguts after inducing transgenes for 10 days. **B.** Nuclear size distribution of *GFP*$^{+}$ cells in control (*esg^{ts}*>+), in *esg^{ts} >yki$^{3S/A}$* midguts, and in *esg^{ts} >yki^{S168A}* midguts at day 10 of transgene induction. **C.** Normalized Nuclear size distribution. Transgenes were induced for 10 days. The data is binned by 4 µm starting from 11 µm. Normalized frequency shows the population sizes relative to the population at 11-15 µm. *GFP*$^{+}$ cells (**C**), N=245 (*esg^{ts}*>+), N=511 (*esg^{ts}>yki$^{3S/A}$*), and N=465 (*esg^{ts}> yki^{S168A}*). A Chi-Square test was performed showing a non-significant difference between *yki$^{3S/A}$* and *yki^{S168A}* cell populations. **D.** Quantification of disseminated cells detected on the surface of posterior midgut at day 10 and day 19.

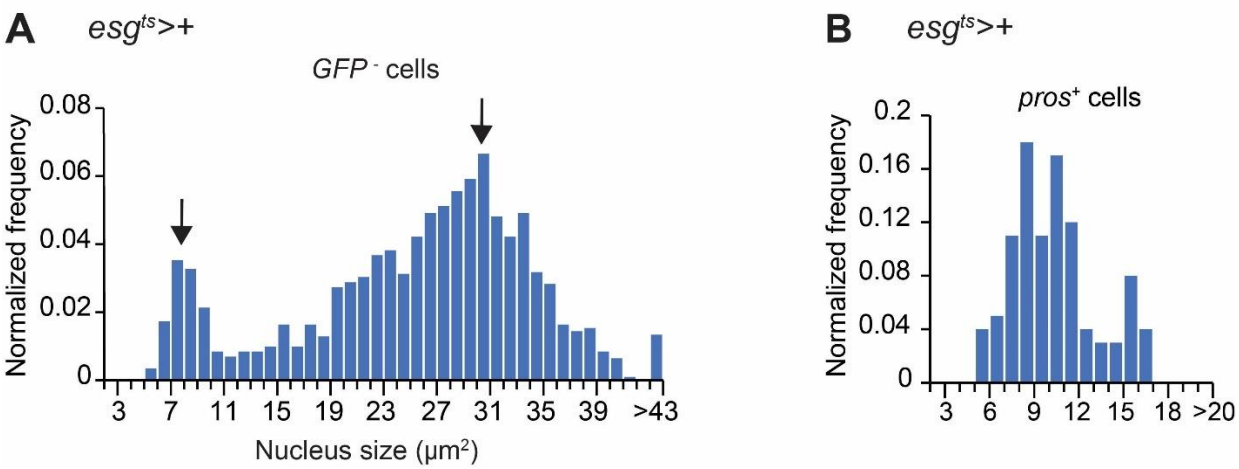

Figure S2. Nuclear size distribution of EEs and ECs in the posterior midguts.

A. Nuclear size distribution of *GFP*$^{-}$ cells (ECs and EEs) in the posterior midguts at day 6. GFP is driven by *esg*^{ts}. Arrows indicate two peaks. N=2013. **B.** Nucleus size distribution of *pros*$^{+}$ cells at day 6. N=100.

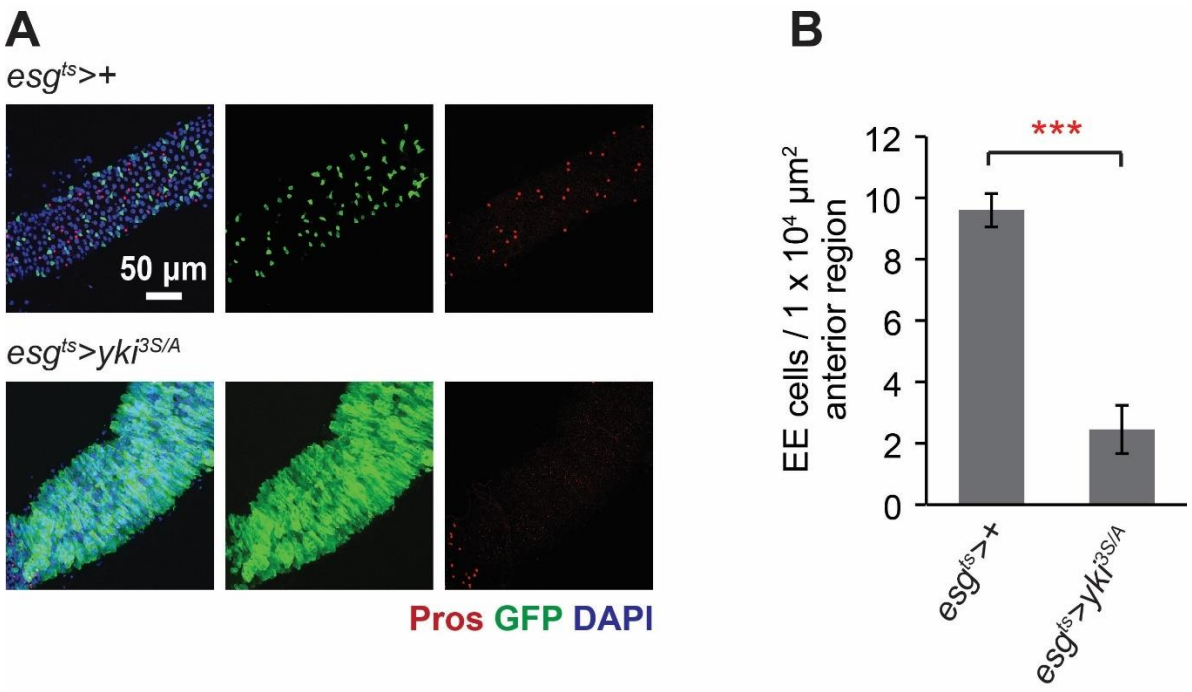

Figure S3. Expression of *yki*$^{3S/A}$ with *esg*^{ts} accumulates cells in EC lineage at the expense of EE lineage.

A. Representative images of Pros staining (red) in the posterior midguts. Transgenes were induced for 8 days. Cells manipulated by *esg*^{ts} are marked with GFP (green). **B.** Quantification of *pros*+ cells in the anterior region of posterior midguts. =15 posterior midguts (*esg*^{ts}>+) and N=20 midguts (*esg*^{ts}>*yki*$^{3S/A}$). Mean±SEMs are shown. ***P<0.01, Mann-Whitney U test.

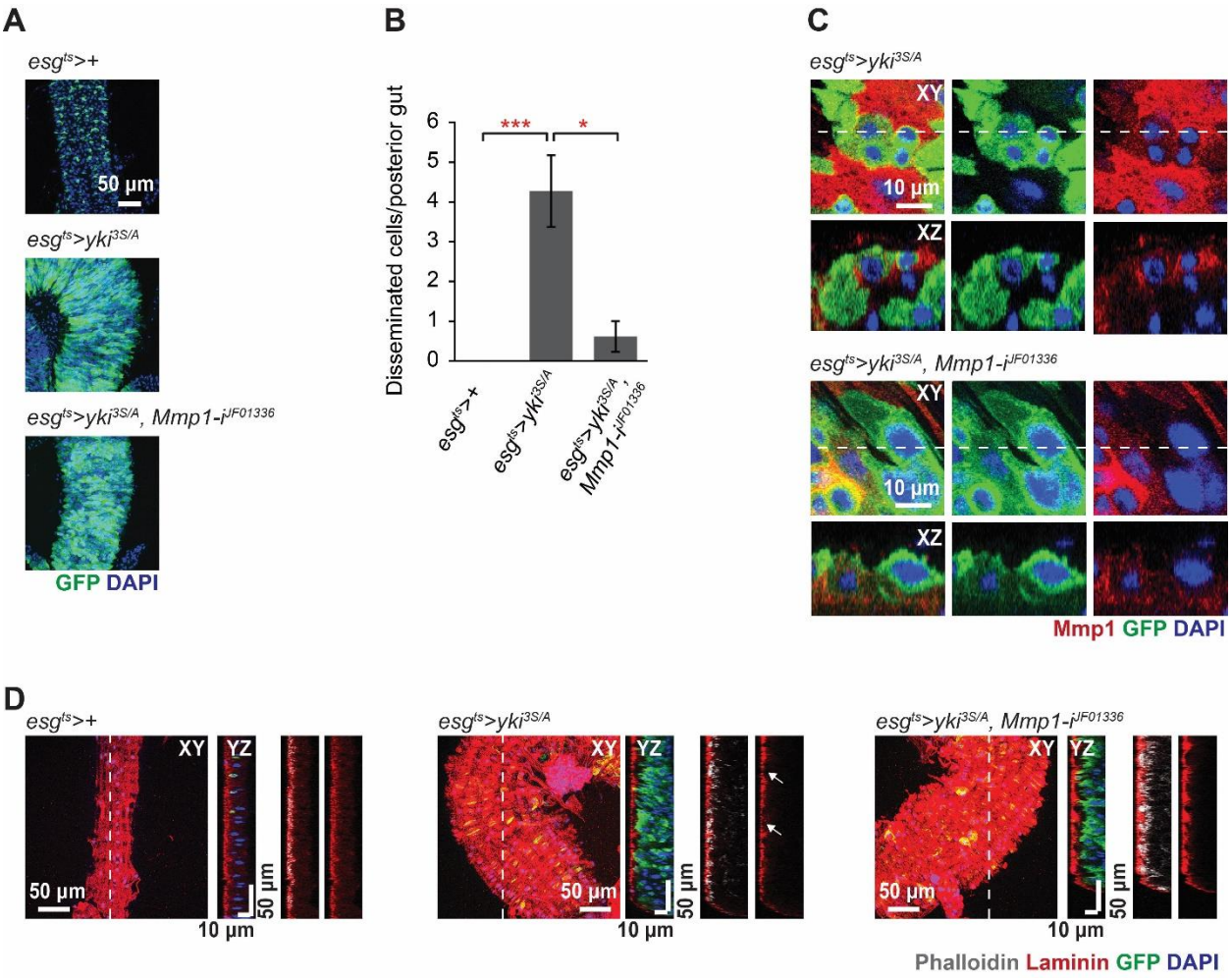

Figure S4. Mmp1 knockdown suppresses the growth of *yki$^{3S/A}$* midgut tumors, leading to the rescue in laminin degradation and the reduction in the number of disseminated *yki$^{3S/A}$* cells.
A. Posterior midguts after inducing transgenes for 12 days. *JF01336* was used to knockdown Mmp1 in *yki$^{3S/A}$* cells. **B.** Quantification of disseminated cells detected on the surface of posterior midgut. **C.** Mmp1 staining (red) at 12 days of transgene(s) induction. **D.** Laminin staining (red) of the midguts. Arrows indicate localized degradation of the laminin layer.

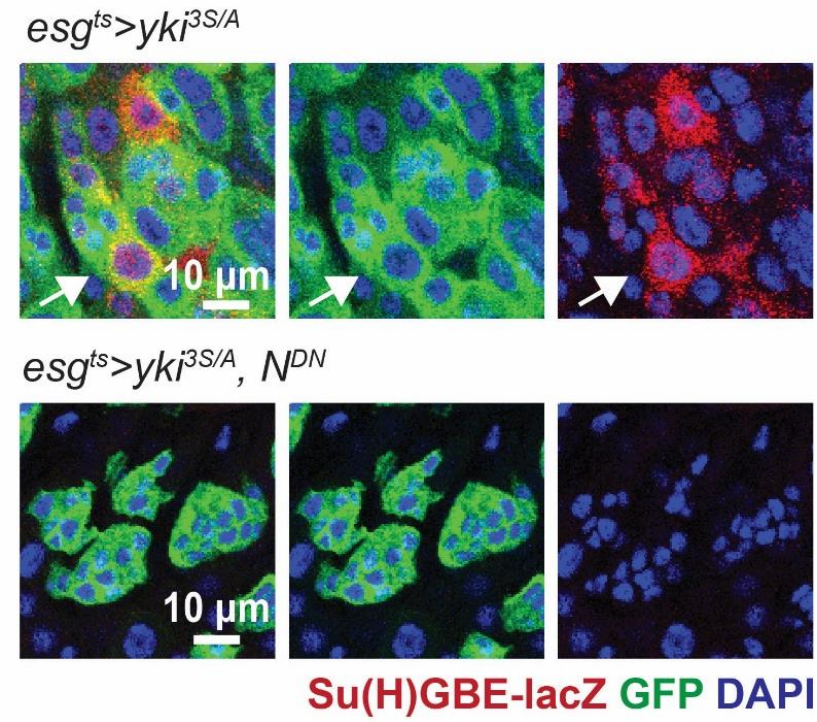

Figure S5. Expression of N^{DN} in $yki^{3S/A}$ cells eliminates EB-like $yki^{3S/A}$ cell population, confirming the inhibition of EC-differentiation in $yki^{3S/A}$ cells.

Su(H)GBE-lacZ signals are shown in red, and $yki^{3S/A}$ and $yki^{3S/A}$, N^{DN} cells are marked by GFP (green). Transgenes were induced for 8 days. Arrow indicates representative GFP^{+} cells with Su(H)GBE-lacZ signals.

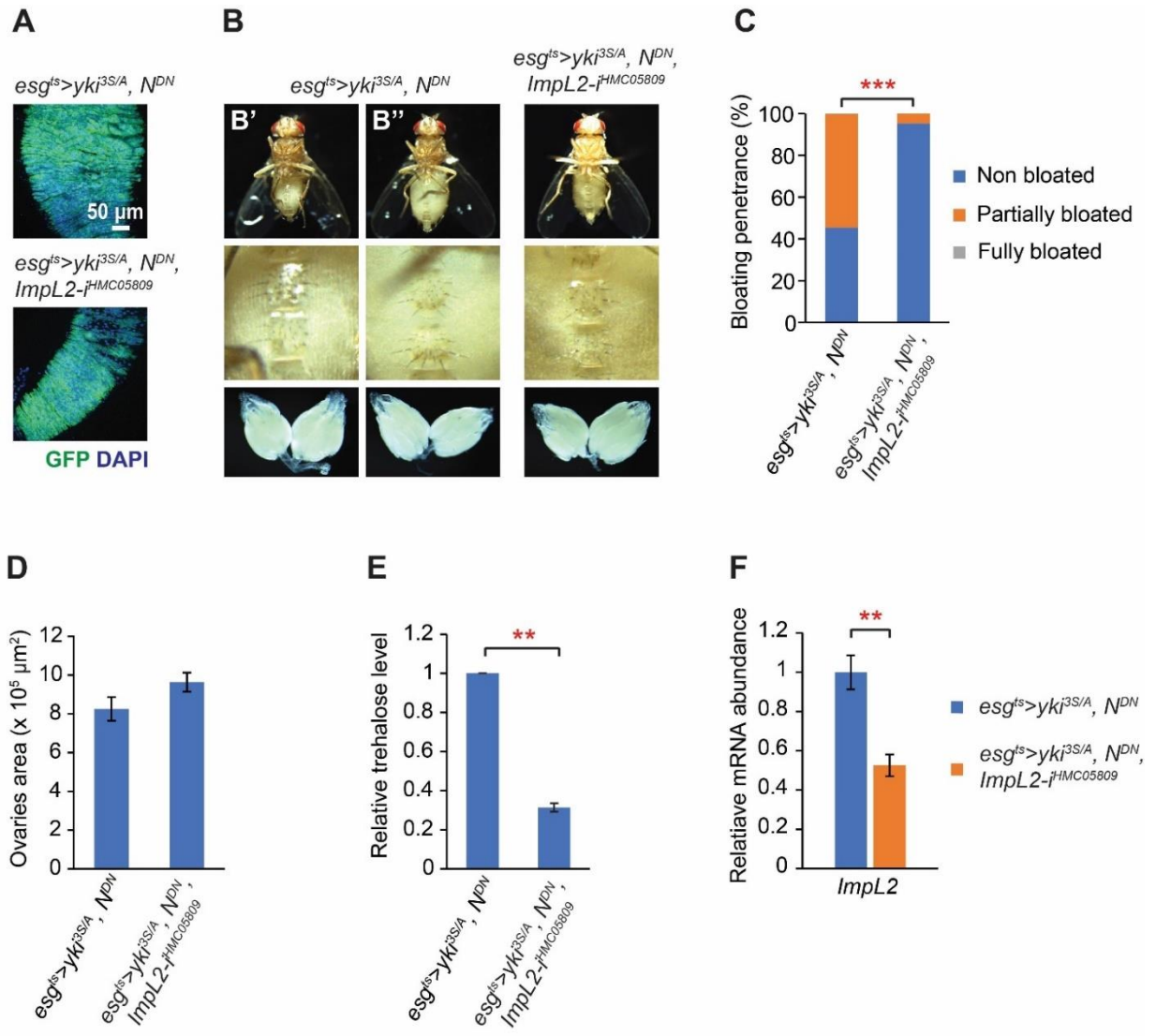

Figure S6. Depletion of *ImpL2* in *yki$^{3S/A}$*, *N^{DN}* tumors further suppresses the wasting phenotypes. **A.** Representative images of *esg^{ts}>yki$^{3S/A}$, N^{DN}* and *esg^{ts}>yki$^{3S/A}$, N^{DN}, ImpL2-i^{HMC05809}* midgut tumors. Transgenes were induced for 8 days. Tumor cells are marked by GFP (green). **B.** Representative ventral views of flies and ovary images. Upper panels, ventral views; middle panels, magnified views of the corresponding fly's abdominal area; lower panels, images of the corresponding fly's ovaries. The upper panels in *esg^{ts}>yki$^{3S/A}$, N^{DN}* show representative non-bloated (normal state) (**B'**) and partially bloated (**B''**) fly's abdominal views. Transgenes were induced for 8 days. **C.** Quantification of bloating syndrome penetrance. Transgenes were induced for 8 days. N=272 animals (*esg^{ts}>yki$^{3S/A}$, N^{DN}*) and N=182 animals (*esg^{ts}>yki$^{3S/A}$, N^{DN}, ImpL2-i^{HMC05809}*). Mean±SEMs are shown. ***P<0.001, chi-square test. **D.** Quantification of ovaries size. N=20 pairs of ovaries) (*esg^{ts}>yki$^{3S/A}$, N^{DN}*) and N=21 pairs of ovaries (*esg^{ts}>yki$^{3S/A}$, N^{DN}, ImpL2-i^{HMC05809}*). Mean±SEMs are shown. Two-tailed unpaired Student's t-test. **E.** Relative trehalose levels in *esg^{ts}>yki$^{3S/A}$, N^{DN}* and *esg^{ts}>yki$^{3S/A}$, N^{DN}, ImpL2-i^{HMC05809}* flies at day 8 of transgene induction. Mean±SEMs are shown. N=6 female flies, 3 biological replicates. **P<0.01, two-tailed unpaired Student's t-test. **F.** Relative *ImpL2* mRNA levels. Depletion of ImpL2 further reduced *ImpL2* mRNA levels in *yki$^{3S/A}$, N^{DN}, ImpL2-i^{HMC05809}* tumors compared to *yki$^{3S/A}$, N^{DN}* tumors. N=10 midguts, 3 biological replicates. **P<0.01, two-tailed unpaired Student's t-test.

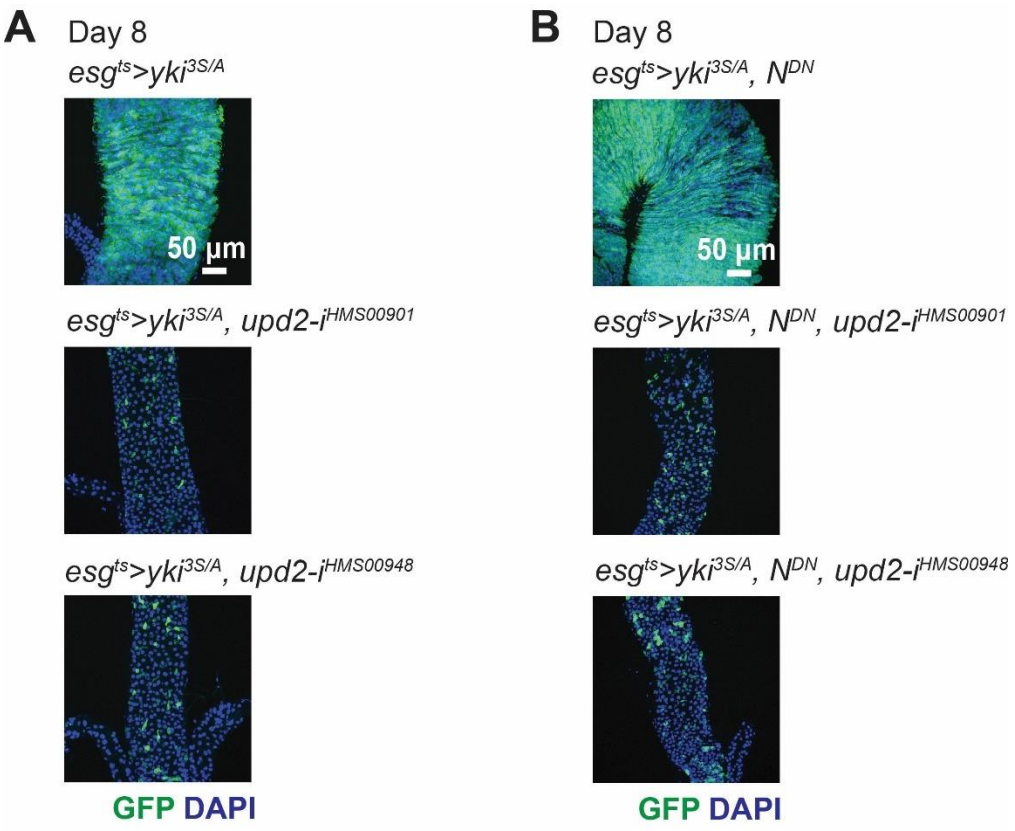

Figure S7. Upd2 expression in *yki$^{3S/A}$* midgut tumor cells and *yki$^{3S/A}$*, *N^{DN}* midgut tumor cells is required for tumor development.

Representative images of the posterior midguts are shown. Two independent *upd2* RNAi lines (*HMS00901* and *HMS00948*) are used to knockdown *upd2* in **A.** *yki$^{3S/A}$* cells and **B.** *yki$^{3S/A}$*, *N^{DN}* cells for 8 days. Requirement of Upd2 in *yki$^{3S/A}$*, *N^{DN}* cells for the tumor development indicates that Upd2 is expressed in the tumor cells.

References

Aalto, A., Olguin-Olguin, A., & Raz, E. (2021). Zebrafish Primordial Germ Cell Migration. In *Frontiers in Cell and Developmental Biology* (Vol. 9). Frontiers Media S.A. https://doi.org/10.3389/fcell.2021.684460

Antonello, Z. A., Reiff, T., Ballesta-Illan, E., & Dominguez, M. (2015). Robust intestinal homeostasis relies on cellular plasticity in enteroblasts mediated by miR-8–Escargot switch. *The EMBO Journal*, *34*(15), 2025–2041. https://doi.org/10.15252/embj.201591517

Antonello, Z. A., Reiff, T., & Dominguez, M. (2015). Mesenchymal to epithelial transition during tissue homeostasis and regeneration: Patching up the Drosophila midgut epithelium. *Fly*, *9*(3), 132–137. https://doi.org/10.1080/19336934.2016.1140709

Apidianakis, Y., Pitsouli, C., Perrimon, N., & Rahme, L. (2009). Synergy between bacterial infection and geneticpredisposition in intestinal dysplasia. *Proceedings of the National Academy of Sciences of the United States of America*, *106*(49), 20883–20888.

Argilés, J. M., Busquets, S., Stemmler, B., & López-Soriano, F. J. (2014). Cancer cachexia: Understanding the molecular basis. In *Nature Reviews Cancer* (Vol. 14, Issue 11, pp. 754–762). Nature Publishing Group. https://doi.org/10.1038/nrc3829

Arvidsson, A., Collin, T., Kirik, D., Kokaia, Z., & Lindvall, O. (2002). Neuronal replacement from endogenous precursors in the adult brain after stroke. *Nature Medicine*, *8*(9), 963–970. https://doi.org/10.1038/nm747

Baracos, V. E., Martin, L., Korc, M., Guttridge, D. C., & Fearon, K. C. H. (2018). Cancer-associated cachexia. In *Nature Reviews Disease Primers* (Vol. 4). Nature Publishing Group. https://doi.org/10.1038/nrdp.2017.105

Beebe, K., Lee, W. C., & Micchelli, C. A. (2010). JAK/STAT signaling coordinates stem cell proliferation and multilineage differentiation in the Drosophila intestinal stem cell lineage. *Developmental Biology*, *338*(1), 28–37. https://doi.org/10.1016/j.ydbio.2009.10.045

Bilder, D., Ong, K., Hsi, T. C., Adiga, K., & Kim, J. (2021). Tumour–host interactions through the lens of Drosophila. In *Nature Reviews Cancer* (Vol. 21, Issue 11, pp. 687–700). Nature Research. https://doi.org/10.1038/s41568-021-00387-5

Biteau, B., & Jasper, H. (2014). Slit/Robo Signaling Regulates Cell Fate Decisions in the Intestinal Stem Cell Lineage of Drosophila. *Cell Reports*, *7*(6), 1867–1875. https://doi.org/10.1016/j.celrep.2014.05.024

Borczuk, A. C., Gorenstein, L., Walter, K. L., Assaad, A. A., Wang, L., & Powell, C. A. (2003). Non-Small-Cell Lung Cancer Molecular Signatures Recapitulate Lung Developmental Pathways. *American Journal of Pathology*, *163*(5), 1949–1960. https://doi.org/10.1016/S0002-9440(10)63553-5

Boumard, B., & Bardin, A. J. (2021). An amuse-bouche of stem cell regulation: Underlying principles and mechanisms from adult Drosophila intestinal stem cells. In *Current Opinion in Cell Biology* (Vol. 73, pp. 58–68). Elsevier Ltd. https://doi.org/10.1016/j.ceb.2021.05.007

Chen, K., Huang, Y. H., & Chen, J. L. (2013). Understanding and targeting cancer stem cells: Therapeutic implications and challenges. In *Acta Pharmacologica Sinica* (Vol. 34, Issue 6, pp. 732–740). https://doi.org/10.1038/aps.2013.27

Cook, J. H., Melloni, G. E. M., Gulhan, D. C., Park, P. J., & Haigis, K. M. (2021). The origins and genetic interactions of KRAS mutations are allele- and tissue-specific. *Nature Communications*, *12*(1). https://doi.org/10.1038/s41467-021-22125-z

Couturier, C. P., Ayyadhury, S., Le, P. U., Nadaf, J., Monlong, J., Riva, G., Allache, R., Baig, S., Yan, X., Bourgey, M., Lee, C., Wang, Y. C. D., Wee Yong, V., Guiot, M. C., Najafabadi, H., Misic, B., Antel, J., Bourque, G., Ragoussis, J., & Petrecca, K. (2020). Single-cell RNA-seq reveals that glioblastoma recapitulates a normal neurodevelopmental hierarchy. *Nature Communications*, *11*(1). https://doi.org/10.1038/s41467-020-17186-5

da Silva-Diz, V., Lorenzo-Sanz, L., Bernat-Peguera, A., Lopez-Cerda, M., & Muñoz, P. (2018). Cancer cell plasticity: Impact on tumor progression and therapy response. *Seminars in Cancer Biology*, *53*(June), 48–58. https://doi.org/10.1016/j.semcancer.2018.08.009

Dong, J., Feldmann, G., Huang, J., Wu, S., Zhang, N., Comerford, S. A., Gayyed, M. F. F., Anders, R. A., Maitra, A., & Pan, D. (2007). Elucidation of a Universal Size-Control Mechanism in Drosophila and Mammals. *Cell*, *130*(6), 1120–1133. https://doi.org/10.1016/j.cell.2007.07.019

Dong, J., Yu, J., Li, Z., Gao, S., Wang, H., Yang, S., Wu, L., Lan, C., Zhao, T., Gao, C., Liu, Z., Wang, X., & Hao, J. (2021). Serum insulin-like growth factor binding protein 2 levels as biomarker for pancreatic ductal adenocarcinoma-associated malnutrition and muscle wasting. *Journal of Cachexia, Sarcopenia and Muscle*, *12*(3), 704–716. https://doi.org/10.1002/jcsm.12692

Figueroa-Clarevega, A., & Bilder, D. (2015). Malignant drosophila tumors interrupt insulin signaling to induce cachexia-like wasting. *Developmental Cell*, *33*(1), 47–55. https://doi.org/10.1016/j.devcel.2015.03.001

Fukuzawa, R., Anaka, M. R., Morison, I. M., & Reeve, A. E. (2017). The developmental programme for genesis of the entire kidney is recapitulated in Wilms tumour. PLoS ONE, 12(10). https://doi.org/10.1371/journal.pone.0186333

Genovese, S., Clé ment, R., Gaultier, C., Besse, F., Narbonne-Reveau, K., Daian, F., Foppolo, S., Miguel Luis, N., & dric Maurange, C. (2019). Coopted temporal patterning governs cellular hierarchy, heterogeneity and metabolism in Drosophila neuroblast tumors. eLife, 8, e50375. https://doi.org/10.7554/eLife.50375.001

Glasheen, B. M., Kabra, A. T., & Page-McCaw, A. (2009). Distinct functions for the catalytic and hemopexin domains of a Drosophila matrix metalloproteinase. *Proceedings of the National Academy of Sciences of the United States of America*, *106*(8), 2659–2664. https://doi.org/10.1073/pnas.0804171106

Goveia, J., Rohlenova, K., Taverna, F., Treps, L., Conradi, L. C., Pircher, A., Geldhof, V., de Rooij, L. P. M. H., Kalucka, J., Sokol, L., García-Caballero, M., Zheng, Y., Qian, J., Teuwen, L. A., Khan, S., Boeckx, B., Wauters, E., Decaluwé, H., De Leyn, P., … Carmeliet, P. (2020). An Integrated Gene Expression Landscape Profiling Approach to Identify Lung Tumor Endothelial Cell Heterogeneity and Angiogenic Candidates. *Cancer Cell*, *37*(1), 21-36.e13. https://doi.org/10.1016/j.ccell.2019.12.001

Hou, S. X., & Singh, S. R. (2017). Stem-Cell-Based Tumorigenesis in Adult Drosophila. In *Current Topics in Developmental Biology* (Vol. 121, pp. 311–337). Academic Press Inc. https://doi.org/10.1016/bs.ctdb.2016.07.013

Howard, A. M., Lafever, K. S., Fenix, A. M., Scurrah, C. R., Lau, K. S., Burnette, D. T., Bhave, G., Ferrell, N., & Page-Mccaw, A. (2019). DSS-induced damage to basement membranes is repaired by matrix replacement and crosslinking. *Journal of Cell Science*, *132*(7). https://doi.org/10.1242/jcs.226860

Hu, D. J. K., Yun, J., Elstrott, J., & Jasper, H. (2021). Non-canonical Wnt signaling promotes directed migration of intestinal stem cells to sites of injury. *Nature Communications*, *12*(1). https://doi.org/10.1038/s41467-021-27384-4

Hwang, N. S., Varghese, S., & Elisseeff, J. (2008). Controlled differentiation of stem cells. In *Advanced Drug Delivery Reviews* (Vol. 60, Issue 2, pp. 199–214). https://doi.org/10.1016/j.addr.2007.08.036

Jiang, H., & Edgar, B. A. (2009). EGFR signaling regulates the proliferation of Drosophila adult midgut progenitors. *Development*, *136*(3), 483–493. https://doi.org/10.1242/dev.026955

Jiang, H., Tian, A., & Jiang, J. (2016). Intestinal stem cell response to injury: lessons from Drosophila. *Cellular and Molecular Life Sciences*, *73*(17), 3337–3349. https://doi.org/10.1007/s00018-016-2235-9

Jögi, A., Vaapil, M., Johansson, M., & Påhlman, S. (2012). Cancer cell differentiation heterogeneity and aggressive behavior in solid tumors. *Upsala Journal of Medical Sciences*, *117*(2), 217–224. https://doi.org/10.3109/03009734.2012.659294

Kelleher, F., Fennelly, D., & Rafferty, M. (2006). Common critical pathways in embryogenesis and cancer. In *Acta Oncologica* (Vol. 45, Issue 4, pp. 375–388). https://doi.org/10.1080/02841860600602946

Kim, J., Chuang, H. C., Wolf, N. K., Nicolai, C. J., Raulet, D. H., Saijo, K., & Bilder, D. (2021). Tumor-induced disruption of the blood-brain barrier promotes host death. *Developmental Cell*, *56*(19), 2712-2721.e4. https://doi.org/10.1016/j.devcel.2021.08.010

Kim, N., Kim, H. K., Lee, K., Hong, Y., Cho, J. H., Choi, J. W., Lee, J. Il, Suh, Y. L., Ku, B. M., Eum, H. H., Choi, S., Choi, Y. La, Joung, J. G., Park, W. Y., Jung, H. A., Sun, J. M., Lee, S. H., Ahn, J. S., Park, K., … Lee, H. O. (2020). Single-cell RNA sequencing demonstrates the molecular and cellular reprogramming of metastatic lung adenocarcinoma. *Nature Communications*, *11*(1). https://doi.org/10.1038/s41467-020-16164-1

Korzelius, J., Naumann, S. K., Loza-Coll, M. A., Chan, J. S., Dutta, D., Oberheim, J., Gläßer, C., Southall, T. D., Brand, A. H., Jones, D. L., & Edgar, B. A. (2014). Escargot maintains stemness and suppresses differentiation in Drosophila intestinal stem cells . *The EMBO Journal*, *33*(24), 2967–2982. https://doi.org/10.15252/embj.201489072

Krakhmal, N. V., Zavyalova, M. V., Denisov, E. V., Vtorushin, S. V., & Perelmuter, V. M. (2015). Cancer invasion: Patterns and mechanisms. *Acta Naturae*, *7*(2), 17–28. https://doi.org/10.32607/20758251-2015-7-2-17-28

Krieger, T., & Simons, B. D. (2015). Dynamic stem cell heterogeneity. In *Development (Cambridge)* (Vol. 142, Issue 8, pp. 1396–1406). Company of Biologists Ltd. https://doi.org/10.1242/dev.101063

Kwon, Y., Song, W., Droujinine, I. A., Hu, Y., Asara, J. M., & Perrimon, N. (2015). Systemic organ wasting induced by localized expression of the secreted Insulin/IGF antagonist ImpL2. *Developmental Cell*, *33*(1), 36–46. https://doi.org/10.1016/j.devcel.2015.02.012

Lawson, D. A., Kessenbrock, K., Davis, R. T., Pervolarakis, N., & Werb, Z. (2018). Tumour heterogeneity and metastasis at single-cell resolution. In *Nature Cell Biology* (Vol. 20, Issue 12, pp. 1349–1360). Nature Publishing Group. https://doi.org/10.1038/s41556-018-0236-7

Lee, J., Cabrera, A. J. H., Nguyen, C. M. T., & Kwon, Y. V. (2020). Dissemination of RasV12-transformed cells requires the mechanosensitive channel Piezo. *Nature Communications*, *11*(3568). https://doi.org/10.1038/s41467-020-17341-y

Lee, J., G-L Ng, K., Dombek, K. M., Seok Eom, D., & Kwon, Y. V. (2021). Tumors overcome the action of the wasting factor ImpL2 by locally elevating Wnt/Wingless. *Proceedings of the National Academy of Sciences of the United States of America*, *118*(23). https://doi.org/10.1073/pnas.2020120118/-/DCSupplemental

Lee, S. H., Park, J. S., Kim, Y. S., Chung, H. Y., & Yoo, M. A. (2012). Requirement of matrix metalloproteinase-1 for intestinal homeostasis in the adult Drosophila midgut. *Experimental Cell Research*, *318*(5), 670–681. https://doi.org/10.1016/j.yexcr.2012.01.004

Li, H., & Jasper, H. (2016). Gastrointestinal stem cells in health and disease: From flies to humans. In *DMM Disease Models and Mechanisms* (Vol. 9, Issue 5, pp. 487–499). Company of Biologists Ltd. https://doi.org/10.1242/dmm.024232

Liu, Y., Saavedra, P., & Perrimon, N. (2022). Cancer cachexia: lessons from Drosophila. In *DMM Disease Models and Mechanisms* (Vol. 15, Issue 3). Company of Biologists Ltd. https://doi.org/10.1242/DMM.049298

Lodge, W., Zavortink, M., Golenkina, S., Froldi, F., Dark, C., Cheung, S., Parker, B. L., Blazev, R., Bakopoulos, D., Christie, E. L., Wimmer, V. C., Duckworth, B. C., Richardson, H. E., & Cheng, L. Y. (2021). Tumor-derived MMPs regulate cachexia in a Drosophila cancer model. *Developmental Cell*, *10(9)*, 491-500.

Lowell, S., Jones, P., Le Roux, I., Dunne, J., & Watt, F. M. (2000). Stimulation of human epidermal differentiation by Delta-Notch signalling at the boundaries of stem-cell clusters. *Current Biology*, *56*(18), 2664-2680.e6. https://doi.org/10.1016/j.devcel.2021.08.008

Loza-Coll, M. A., Southall, T. D., Sandall, S. L., Brand, A. H., & Jones, D. L. (2014). Regulation of Drosophila intestinal stem cell maintenance and differentiation by the transcription factor Escargot . *The EMBO Journal*, *33*(24), 2983–2996. https://doi.org/10.15252/embj.201489050

Ma, X., Chen, Y., Xu, W., Wu, N., Li, M., Cao, Y., Wu, S., Li, Q., & Xue, L. (2015). Impaired Hippo signaling promotes Rho1-JNK-dependent growth. *Proceedings of the National Academy of Sciences of the United States of America*, *112*(4), 1065–1070. https://doi.org/10.1073/pnas.1415020112

Markstein, M., Dettorre, S., Cho, J., Neumüller, R. A., Craig-Müller, S., & Perrimon, N. (2014). Systematic screen of chemotherapeutics in Drosophila stem cell tumors. *Proceedings of the National Academy of Sciences of the United States of America*, *111*(12), 4530–4535. https://doi.org/10.1073/pnas.1401160111

Martín-Blanco, E., Gampel, A., Ring, J., Virdee, K., Kirov, N., Tolkovsky, A. M., & Martinez-Arias, A. (1998). puckered encodes a phosphatase that mediates a feedback loop regulating JNK activity during dorsal closure in *Drosophila*. *Genes & Development*, *12*, 557–570.

Micchelli, C. A., & Perrimon, N. (2006). Evidence that stem cells reside in the adult Drosophila midgut epithelium. *Nature*, *439*(7075), 475–479. https://doi.org/10.1038/nature04371

Miguel-Aliaga, I., Jasper, H., & Lemaitre, B. (2018). Anatomy and physiology of the digestive tract of drosophila melanogaster. *Genetics*, *210*(2), 357–396. https://doi.org/10.1534/genetics.118.300224

Montell, D. J. (2003). Border-cell migration: The race is on. *Nature Reviews Molecular Cell Biology*, *4*(1), 13–24. https://doi.org/10.1038/nrm1006

Oh, H., & Irvine, K. D. (2009). In vivo analysis of Yorkie phosphorylation sites. *Oncogene*, *28*(17), 1916–1927. https://doi.org/10.1038/onc.2009.43

Ohlstein, B., & Spradling, A. (2006). The adult Drosophila posterior midgut is maintained by pluripotent stem cells. *Nature*, *439*(7075), 470–474. https://doi.org/10.1038/nature04333

Pagliarini, R. A., & Xu, T. (2003). A Genetic Screen in Drosophila for Metastatic Behavior. *Science*, *302*(5648), 1227–1231. https://doi.org/10.1126/science.1088474

Pan, D. (2010). The hippo signaling pathway in development and cancer. In *Developmental Cell* (Vol. 19, Issue 4, pp. 491–505). https://doi.org/10.1016/j.devcel.2010.09.011

Pandya, P., Orgaz, J. L., & Sanz-Moreno, V. (2017). Modes of invasion during tumour dissemination. *Molecular Oncology*, *11*(1), 5–27. https://doi.org/10.1002/1878-0261.12019

Parent, J. M., Valentin, V. V, & Lowenstein, D. H. (2002). Prolonged Seizures Increase Proliferating Neuroblasts in the Adult Rat Subventricular Zone-Olfactory Bulb Pathway. *The Journal of Neuroscience*, 22(8), 3174–3188.

Peercy, B. E., & Starz-Gaiano, M. (2020). Clustered cell migration: Modeling the model system of Drosophila border cells. *Seminars in Cell and Developmental Biology*, *100*(December 2019), 167–176. https://doi.org/10.1016/j.semcdb.2019.11.010

Petruzzelli, M., & Wagner, E. F. (2016). Mechanisms of metabolic dysfunction in cancer-associated cachexia. *Genes & Development*, *30*, 489–501. https://doi.org/10.1101/gad.276733

Porporato, P. E. (2016). Understanding cachexia as a cancer metabolism syndrome. In *Oncogenesis* (Vol. 5, Issue 2). Nature Publishing Group. https://doi.org/10.1038/oncsis.2016.3

Rangarajan, A., Talora, C., Okuyama, R., Nicolas, M., Mammucari, C., Oh, H., Aster, J. C., Krishna, S., Metzger, D., Chambon, P., Miele, L., Aguet, M., Radtke, F., & Dotto, G. P. (2001). Notch signaling is a direct determinant of keratinocyte growth arrest and entry into differentiation. *EMBO Journal*, *20*(13), 3427–3436. https://doi.org/10.1093/emboj/20.13.3427

Rojas Villa, S. E., Meng, F. W., & Biteau, B. (2019). Zfh2 controls progenitor cell activation and differentiation in the adult Drosophila intestinal absorptive lineage. *PLoS Genetics*, *15*(12), 1–24. https://doi.org/10.1371/journal.pgen.1008553

Song, W., Kir, S., Hong, S., Hu, Y., Wang, X., Binari, R., Tang, H. W., Chung, V., Banks, A. S., Spiegelman, B., & Perrimon, N. (2019). Tumor-Derived Ligands Trigger Tumor Growth and Host Wasting via Differential MEK Activation. *Developmental Cell*, *48*(2), 277-286.e6. https://doi.org/10.1016/j.devcel.2018.12.003

Stevens, L. J., & Page-McCaw, A. (2012). A secreted MMP is required for reepithelialization during wound healing. *Molecular Biology of the Cell*, *23*(6), 1068–1079. https://doi.org/10.1091/mbc.E11-09-0745

Tu, B., Yao, J., Ferri-Borgogno, S., Zhao, J., Chen, S., Wang, Q., Yan, L., Zhou, X., Zhu, C., Bang, S., Chang, Q., Bristow, C. A., Kang, Y., Zheng, H., Wang, H., Fleming, J. B., Kim, M., Heffernan, T. P., Draetta, G. F., … Ying, H. (2019). YAP1 oncogene is a context-specific driver for pancreatic ductal adenocarcinoma. *Journal of Clinical Investigation Insight*, *4*(21). https://doi.org/10.1172/jci.insight.130811

Uhlirova, M., & Bohmann, D. (2006). JNK- and Fos-regulated Mmp1 expression cooperates with Ras to induce invasive tumors in Drosophila. *EMBO Journal*, *25*(22), 5294–5304. https://doi.org/10.1038/sj.emboj.7601401

Vasilyev, A., Liu, Y., Mudumana, S., Mangos, S., Lam, P. Y., Majumdar, A., Zhao, J., Poon, K. L., Kondrychyn, I., Korzh, V., & Drummond, I. A. (2009). Collective cell migration drives morphogenesis of the kidney nephron. *PLoS Biology*, *7*(1). https://doi.org/10.1371/journal.pbio.1000009

Villegas, S. N. (2019). One hundred years of Drosophila cancer research: No longer in solitude. *DMM Disease Models and Mechanisms*, *12*(4). https://doi.org/10.1242/dmm.039032

Wang, C., Yin, M. X., Wu, W., Dong, L., Wang, S., Lu, Y., Xu, J., Wu, W., Li, S., Zhao, Y., & Zhang, L. (2016). Taiman acts as a coactivator of Yorkie in the Hippo pathway to promote tissue growth and intestinal regeneration. *Cell Discovery*, *2*, 1–15. https://doi.org/10.1038/celldisc.2016.6

Weng, A. P., Millholland, J. M., Yashiro-Ohtani, Y., Arcangeli, M. L., Lau, A., Wai, C., Del Bianco, C., Rodriguez, C. G., Sai, H., Tobias, J., Li, Y., Wolfe, M. S., Shachaf, C., Felsher, D., Blacklow, S. C.,

Pear, W. S., & Aster, J. C. (2006). c-Myc is an important direct target of Notch1 in T-cell acute lymphoblastic leukemia/lymphoma. *Genes and Development*, *20*(15), 2096–2109. https://doi.org/10.1101/gad.1450406

Wittkorn, E., Sarkar, A., Garcia, K., Kango-Singh, M., & Singh, A. (2015). The Hippo pathway effector Yki downregulates Wg signaling to promote retinal differentiation in the Drosophila eye. *Development (Cambridge)*, *142*(11), 2002–2013. https://doi.org/10.1242/dev.117358

Wu, F., Fan, J., He, Y., Xiong, A., Yu, J., Li, Y., Zhang, Y., Zhao, W., Zhou, F., Li, W., Zhang, J., Zhang, X., Qiao, M., Gao, G., Chen, S., Chen, X., Li, X., Hou, L., Wu, C., … Zhou, C. (2021). Single-cell profiling of tumor heterogeneity and the microenvironment in advanced non-small cell lung cancer. *Nature Communications*, *12*(1). https://doi.org/10.1038/s41467-021-22801-0

Yang, S. A., Portilla, J. M., Mihailovic, S., Huang, Y. C., & Deng, W. M. (2019). Oncogenic Notch Triggers Neoplastic Tumorigenesis in a Transition-Zone-like Tissue Microenvironment. *Developmental Cell*, *49*(3), 461-472.e5. https://doi.org/10.1016/j.devcel.2019.03.015

Yeo, S. K., Zhu, X., Okamoto, T., Hao, M., Wang, C., Lu, P., Lu, L. J., & Guan, J. L. (2020). Single-cell RNA-sequencing reveals distinct patterns of cell state heterogeneity in mouse models of breast cancer. *ELife*, *9*, 1–24. https://doi.org/10.7554/ELIFE.58810

Yeom, E., Shin, H., Yoo, W., Jun, E., Kim, S., Hong, S. H., Kwon, D. W., Ryu, T. H., Suh, J. M., Kim, S. C., Lee, K. S., & Yu, K. (2021). Tumour-derived Dilp8/INSL3 induces cancer anorexia by regulating feeding neuropeptides via Lgr3/8 in the brain. *Nature Cell Biology*, *23*(2), 172–183. https://doi.org/10.1038/s41556-020-00628-z

Zakrzewski, W., Dobrzyński, M., Szymonowicz, M., & Rybak, Z. (2019). Stem cells: Past, present, and future. In *Stem Cell Research and Therapy* (Vol. 10, Issue 1). BioMed Central Ltd. https://doi.org/10.1186/s13287-019-1165-5

Zeng, X., & Hou, S. X. (2015). Enteroendocrine cells are generated from stem cells through a distinct progenitor in the adult drosophila posterior midgut. *Development (Cambridge)*, *142*(4), 644–653. https://doi.org/10.1242/dev.113357

Zhai, Z., Kondo, S., Ha, N., Boquete, J. P., Brunner, M., Ueda, R., & Lemaitre, B. (2015). Accumulation of differentiating intestinal stem cell progenies drives tumorigenesis. *Nature Communications*, *6*. https://doi.org/10.1038/ncomms10219